Geomechanics and Engineering, *Vol. 28, No. 5 (2022) 437-454*
https://doi.org/10.12989/gae.2022.28.5.437

Geomechanical and hydrogeological validation of hydro-mechanical two-way sequential coupling in TOUGH2-FLAC3D linking algorithm with insights into the Mandel, Noordbergum, and Rhade effects

Sungho Lee[1], Jai-Yong Park[2], Jung-Hwi Kihm[3] and Jun-Mo Kim[*1,4]

[1]*School of Earth and Environmental Sciences, Seoul National University, Seoul 08826, Republic of Korea*
[2]*Geology Division, Korea Institute of Geoscience and Mineral Resources, Daejeon 34132, Republic of Korea*
[3]*Department of Fire and Disaster Prevention, Jungwon University, Goesan-Gun 28024, Republic of Korea*
[4]*GeoLab, Seoul 08787, Republic of Korea*

(Received March 29, 2021, Revised December 9, 2021, Accepted December 13, 2021)

Abstract. The hydro-mechanical (HM) two-way sequential coupling in the TOUGH2-FLAC3D linking algorithm is validated completely and successfully in both M to H and H to M directions, which are initiated by mechanical surface loading for geomechanical validation and hydrological groundwater pumping for hydrogeological validation, respectively. For such complete and successful validation, a TOUGH2-FLAC3D linked numerical model is developed first by adopting the TOUGH2-FLAC3D linking algorithm, which uses the two-way (fixed-stress split) sequential coupling scheme and the implicit backward time stepping method. Two geomechanical and two hydrogeological validation problems are then simulated using the linked numerical model together with basic validation strategies and prerequisites. The second geomechanical and second hydrogeological validation problems are also associated with the Mandel effect and the Noordbergum and Rhade effects, respectively, which are three phenomenally well-known but numerically challenging HM effects. Finally, sequentially coupled numerical solutions are compared with either analytical solutions (verification) or fully coupled numerical solutions (benchmarking). In all the four validation problems, they show almost perfect to extremely or very good agreement. In addition, the second geomechanical validation problem clearly displays the Mandel effect and suggests a proper or minimum geometrical ratio of the height to the width for the rectangular domain to maximize agreement between the numerical and analytical solutions. In the meantime, the second hydrogeological validation problem clearly displays the Noordbergum and Rhade effects and implies that the HM two-way sequential coupling scheme used in the linked numerical model is as rigorous as the HM two-way full coupling scheme used in a fully coupled numerical model.

Keywords: geomechanical validation; hydrogeological validation; hydro-mechanical two-way sequential coupling; Mandel effect; Noordbergum effect; Rhade effect; TOUGH2-FLAC3D linking algorithm

1. Introduction

Aboustit *et al*. (1982) and Noorishad *et al*. (1984) first presented fully coupled single-phase thermo-hydro-mechanical (THM) formulations and codes for geologic media (i.e., soils and rocks). Although their efforts have drawn attention to development of more complicate, fully coupled multi-phase THM formulations and codes, it has still been difficult and tedious to develop a single fully coupled multi-phase THM code. Instead of developing such a single fully coupled multi-phase THM code, Rutqvist *et al*. (2002) first introduced an alternative, which combines two preexisting well established and widely applied individual TH and M codes. In particular, they linked (i.e., sequentially coupled) the multi-phase TH code TOUGH2 (Pruess 1991, Pruess *et al*. 1999, 2012) and the single-phase M code FLAC3D (Itasca Consulting Group 1997, 2009, 2017) and developed the first TOUGH2-linked multi-phase THM code, which was named TOUGH-FLAC. TOUGH2 provides many versatile equation of state (EOS) modules for various fluids and fluid mixtures (water, air, carbon dioxide, hydrogen, methane, nitrogen, oil, and others). Thus, TOUGH2-linked (based) geomechanical numerical models can have the advantage of high applicability to numerous geomechanical and hydrogeological reservoir projects related to such various fluids and fluid mixtures in comparison with other coupled or linked THM simulators (e.g., Olivella *et al*. 1996, Rutqvist *et al*. 2001, Kolditz *et al*. 2012, Dassault Systèmes Simulia 2014, COMSOL 2021).

Rutqvist *et al*.'s (2002) original TOUGH2-FLAC3D linking approach has encouraged many researchers to link the TH code TOUGH2 (Pruess 1991, Pruess *et al*. 1999, 2012) or even thermo-hydro-chemical (THC) code TOUGHREACT (Xu *et al*. 2004, 2006, 2012, 2014) with the M codes such as FLAC3D (Itasca Consulting Group 1997, 2009, 2017) and others. As a result, various TOUGH2- and TOUGHREACT-linked geomechanical numerical models (e.g., Table 1 in Rutqvist (2017)) have been developed and applied actively as follows: TOUGH-

*Corresponding author, Ph.D.
E-mail: junmokim@snu.ac.kr

ISSN: 2005-307X (Print), 2092-6219 (Online)

FLAC (Rutqvist *et al*. 2002, Rutqvist and Tsang 2003, Rutqvist 2011), TOUGHREACT-FLAC3D (Taron *et al*. 2006, Taron 2009, Taron *et al*. 2009, Taron and Elsworth 2010), TOUGH2-BIOT2 (Hurwitz *et al*. 2007, Hutnak *et al*. 2009), TOUGH2-EGS (Fakcharoenphol *et al*. 2012, 2013, Hu *et al*. 2013), TOUGH2-CSM (THM-CO2) (Winterfeld *et al*. 2012, Winterfeld and Wu 2013, Huang *et al*. 2015, Winterfeld and Wu 2015, 2016), TOUGHREACT-ROCMECH (Kim *et al*. 2012a, 2012b, 2015), TOUGH+ HYDRATE-FLAC3D (Kim *et al*. 2012c), TOUGH+ RealGasH2O-ROCMECH (Kim and Moridis 2013, 2014), TOUGH-RDCA (Pan *et al*. 2013, 2014a, 2014b), TOUGH-UDEC (Lee *et al*. 2015a), TOUGH2BIOT (Lei *et al*. 2015), FLAC3D-TOUGH2 (Kwon and Lee 2018), and more others.

In developing the linked numerical models, four different schemes have been presented and adopted for the THM sequential coupling or linking (i.e., TOUGH2-FLAC3D linking algorithm) between the TH(C) TOUGH family codes (i.e., TOUGH2, TOUGHREACT, and others) and M codes (i.e., FLAC3D and others) as follows: one-way (TH to M), two-way (undrained split), two-way (fixed-stress split), and two-way (monolithic) sequential coupling schemes. Such development studies have shown that the THM two-way sequential coupling schemes are numerically more rigorous but more complicate than the THM one-way sequential coupling scheme.

Although the above-mentioned TH(C) TOUGH family codes and M codes are well established and widely applied, these two numerically distinct groups of codes do not assemble inherently a single matrix for all the T, H, M, and C governing equations. Thus, the unknowns (i.e., temperature, multi-phase fluid pressures, displacement vector, and multi-species concentrations) are solved respectively or sequentially in each corresponding code. It raises questions about the integrity (i.e., stability and accuracy) of the TOUGH2-FLAC3D linking algorithm and thus the TOUGH2- and TOUGHREACT-linked geomechanical numerical models as single codes. As a result, validation (i.e., verification and benchmarking) of the linking algorithm and linked numerical models is very crucial and essential as much as their development and application even though they have already been well established and widely applied.

The previous validation studies (e.g., Table 1 in Rutqvist (2017)) have been verified by using three different sets of analytical solutions for mechanical surface loading-induced one-dimensional HM consolidation problems (Terzaghi 1925, Biot 1941), mechanical surface loading-induced two-dimensional HM consolidation problems (Mandel 1953, Abousleiman *et al*. 1996), which are associated with a phenomenally well-known but numerically challenging HM effect (i.e., Mandel effect), and thermal surface heating-induced one-dimensional TM expansion problems (Carslaw and Jaeger 1959, Jaeger *et al*. 2007). However, these previous one- and two-dimensional geomechanical validation studies for the HM one- and two-way sequential coupling have their own limits and shortcomings in terms of two major aspects.

First, in the previous two-dimensional geomechanical validation studies for the HM two-way sequential coupling, the numerical solutions were not exactly or closely identical to the analytical solutions for the Mandel effect, but neither clear explanations nor even explicit descriptions were provided. Thus, revisiting and resolving the mechanical surface loading-induced two-dimensional HM consolidation problems is highly necessary to achieve more successful validation of the HM two-way sequential coupling with respect to the Mandel effect. In addition, the HM one-way sequential coupling cannot produce the Mandel effect at all, and thus it has not been validated by using the analytical solutions for the mechanical surface loading-induced two-dimensional HM consolidation problems (Mandel 1953, Abousleiman *et al*. 1996).

Second, solving the mechanical surface loading-induced one- and two-dimensional HM consolidation problems can play solely as geomechanical validation by initiating the HM coupling in the one direction from the M governing equation to the H governing equation. This one-directional geomechanical (M to H) validation also raises questions about the opposite-directional hydrogeological (H to M) validation because the TOUGH2-FLAC3D linking algorithm does not formulate inherently a single matrix for the H and M governing equations, and thus the unknowns (i.e., multi-phase fluid pressures and displacement vector) cannot be solved simultaneously as mentioned above. In other words, successful mechanical surface loading-induced one-directional geomechanical (M to H) validation cannot guarantee deductively one hundred percent at all successful hydrological fluid pumping or injection-induced opposite-directional hydrogeological (H to M) validation before confirming visually uncontroversial results. Furthermore, the linking algorithm and linked numerical models have mainly been applied to various hydrological fluid pumping and injection-related projects rather than mechanical loading-related projects. Nevertheless, this hydrogeological validation issue has been totally unconcerned so far. Thus, solving hydrological fluid pumping or injection-induced HM consolidation problems is also highly required as hydrogeological validation by initiating the HM coupling in the opposite direction from the H governing equation to the M governing equation. This study will be much more contributive if such hydrogeological validation problems are also associated with other phenomenally well-known but numerically challenging HM effects (e.g., Noordbergum and Rhade effects), which are comparable to the Mandel effect. Performing successfully both geomechanical and hydrogeological validation can verify and justify the stability and accuracy of the HM two-way sequential coupling in both directions between the H and M governing equations.

The objective of this study is to validate the HM two-way sequential coupling in the TOUGH2-FLAC3D linking algorithm completely and successfully in both M to H and H to M directions, which are initiated by mechanical surface loading in one M to H direction for geomechanical validation and hydrological groundwater pumping in opposite H to M direction for hydrogeological validation, respectively. For such complete and successful validation, a TOUGH2-FLAC3D linked numerical model is developed

first by adopting the TOUGH2-FLAC3D linking algorithm, which has been implemented in all the preexisting TOUGH2- and TOUGHREACT-linked geomechanical numerical models (Section 2). A series of four HM consolidation (i.e., groundwater flow and land deformation) problems is then simulated using the linked numerical model (Section 2) together with basic validation strategies and prerequisites (Section 3). The former two are geomechanical validation problems induced by surface loading (Sections 4.1 and 4.2), and the latter two are hydrogeological validation problems caused by groundwater pumping (Sections 5.1 and 5.2). In particular, the second geomechanical and second hydrogeological validation problems are also associated with the Mandel effect and the Noordbergum and Rhade effects, respectively, which are mentioned above as three phenomenally well-known but numerically challenging HM effects. Finally, sequentially coupled numerical solutions are compared with either analytical solutions (verification) (Sections 4.1, 4.2, and 5.1) or fully coupled numerical solutions (benchmarking) (Section 5.2). Contributions and implications of this study are further discussed (Section 6).

2. TOUGH2-FLAC3D linking algorithm

A TOUGH2-FLAC3D linked numerical model, which is named TOUGH2-FLAC3D THM (Lee *et al*. 2015b), is developed independently by adopting the TOUGH2-FLAC3D linking algorithm, which has been implemented in all the preexisting TOUGH2- and TOUGHREACT-linked geomechanical numerical models (e.g., Table 1 in Rutqvist (2017)). In such TOUGH2-FLAC3D linking algorithm, the two-way sequential coupling scheme (Rutqvist *et al*. 2002, Rutqvist and Tsang 2003, Rutqvist 2011, Kim *et al*. 2012a, 2012b, 2015) and the implicit backward time stepping method with the fixed-stress split scheme (Kim 2010, Kim *et al*. 2011a, 2011b) are used because they have been proven to be numerically more accurate and stable than any other sequential coupling schemes and time stepping methods. The key features of the two-way sequential coupling scheme and the implicit backward time stepping method with the fixed-stress split scheme are summarized in Appendices A and B, respectively.

3. Basic validation strategies and prerequisites

In the following two geomechanical (Sections 4.1 and 4.2) and two hydrogeological (Sections 5.1 and 5.2) validation problems for the HM two-way sequential coupling in the TOUGH2-FLAC3D linking algorithm, the thermophysical material properties (i.e., compressibility β_w, dynamic viscosity μ_w, density ρ_w, and unit weight γ_w) of water are assumed to be constant, not variable in space and time. It is accomplished by not using (i.e., by bypassing) any EOS module in TOUGH2. Such constant material properties of water are given as follows: β_w = 4.50 × 10^{-10} m^2/N, μ_w = 10^{-3} kg/m/sec, ρ_w = 10^3 kg/m^3, and $\gamma_w = \rho_w g$ = 9.81 × 10^3 N/m^3 with the gravitational acceleration constant g = 9.81 m/sec^2 (Freeze and Cherry 1979, Domenico and Schwartz 1990). In addition, except for the porosity n, intrinsic permeability tensor $\boldsymbol{k} = k_{ij}$, elastic modulus tensor $\boldsymbol{D} = D_{ijkl}$, and Biot's hydro-mechanical coupling coefficient tensor $\boldsymbol{\alpha}_c = \alpha_{c\,ij}$ of the solid skeleton for the subscripts $i, j, k, l = x, y, z$ and the density ρ_s of the solid grain, all the other material properties of the water, solid grain, and solid skeleton associated with the general multi-phase thermoporoelastic T, H, and M governing equations (e.g., Eqs. (13), (14), (19), and (21) in Rutqvist *et al*. (2001)) are neglected and assumed to be zero in order to deactivate the TM and TH two-way sequential coupling.

4. Geomechanical validation

4.1 Surface loading on a columnar domain

As the first geomechanical validation problem, groundwater flow and land deformation (i.e., HM consolidation) in a saturated column due to mechanical surface loading, which are illustrated in Fig. 1, are simulated using the linked numerical model. Such sequentially coupled HM numerical solutions are then compared and validated with HM analytical solutions (verification).

The physical settings including the assumptions and the initial and boundary conditions for this geomechanical validation problem are described in Appendix C. For such a case, Terzaghi (1925), Biot (1941), and Kim (2000) also derived a set of HM analytical solutions for the excess pore water pressure P_{ex} and vertical displacement u_z.

The height H of the column (i.e., shaded area) is set equal to 10 m in this geomechanical validation problem (Fig. 1). Surface loading is applied on the top boundary (z = 10 m) at an instantaneous and constant total vertical normal stress σ_z = -10^6 N/m^2 (Pa). The material properties of the column (fine sand) are obtained from the literature (Domenico and Schwartz 1990, Das 1994, Kim 2000) and

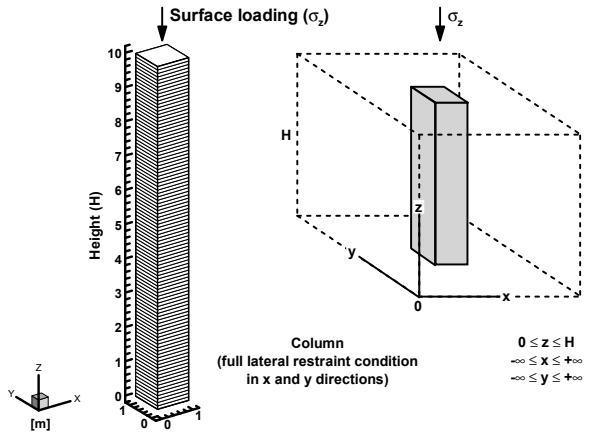

Fig. 1 Schematic diagram of the saturated column under surface loading and grid blocks used in the first geomechanical validation problem

Table 1 Material properties of the fine sand used in the first and second geomechanical validation problems

Property [unit]	Fine sand (column or rectangle)
Porosity n [-]	0.30
Intrinsic permeability k [m^2]	1.02×10^{-12}
Saturated hydraulic conductivity K_{sat} [m/sec]	1.00×10^{-5}
Poisson's ratio ν [-]	0.25
Young's modulus E [Pa]	1.00×10^{7}
Biot's hydro-mechanical coupling coefficient α_c [-]	1.00
Solid density ρ_s [kg/m^3]	2.65×10^{3}

are summarized in Table 1. The initial pore water pressure P_o at the bottom boundary (z = 0 m) is assigned to be equal to the height of the column multiplied by the unit weight of water (i.e., $P_o = H \times \gamma_w$ = 10 m × 9.81 × 10^3 N/m^3 = 9.81 × 10^4 N/m^2). The spatial and temporal discretizations used in the numerical simulation are described in Appendix C.

The sequentially coupled HM numerical solutions are plotted in Fig. 2 and compared with the HM analytical solutions (Terzaghi 1925, Biot 1941, Kim 2000). As shown in Fig. 2, the numerical and analytical solutions show almost perfect agreement for both excess pore water pressure P_{ex} and vertical displacement u_z. In Figs. 2(a) and 2(b), the coefficients of determination R^2 between the analytical and numerical solutions are 0.999 and 0.998 for the temporal changes of the excess pore water pressure and vertical displacement, respectively. In Figs. 2(c) and 2(d), the R^2 between the analytical and numerical solutions are 0.999 and 0.998 for the spatial distributions of the excess pore water pressure and vertical displacement, respectively.

4.2 Surface loading on a rectangular domain: Mandel effect

As the second geomechanical validation problem, groundwater flow and land deformation (i.e., HM consolidation) and the so-called Mandel effect in a saturated rectangle due to mechanical surface loading, which are illustrated in Fig. 3, are simulated using the linked numerical model. Such sequentially coupled HM numerical solutions are then compared and validated with HM analytical solutions (verification).

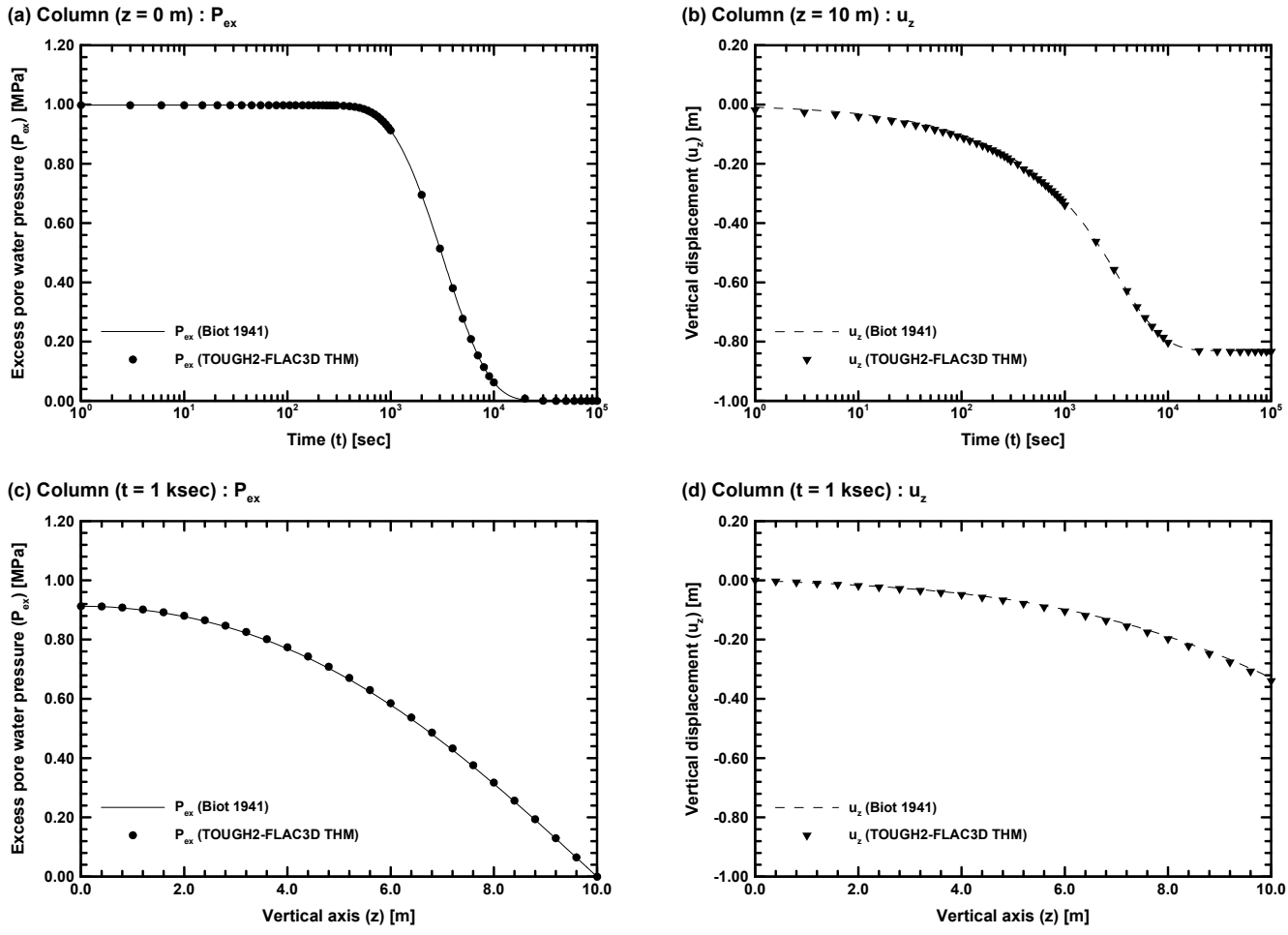

Fig. 2 Temporal changes (upper row) and spatial distributions (lower row) of (a) and (c) excess pore water pressure and (b) and (d) vertical displacement in the saturated column under surface loading

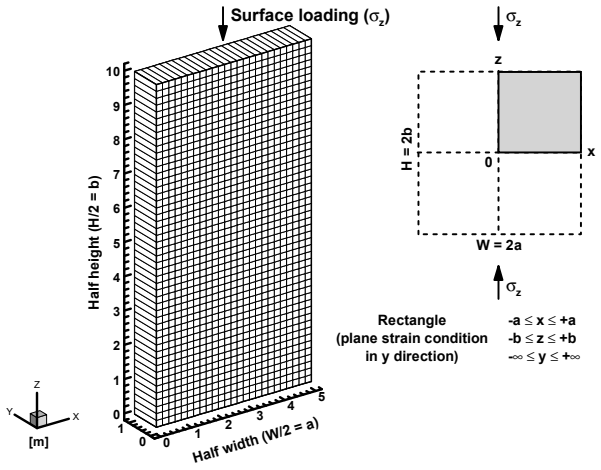

Fig. 3 Schematic diagram of the saturated rectangle under surface loading and grid blocks used in the second geomechanical validation problem

The Mandel effect is a phenomenally well-known but numerically challenging HM effect because it cannot be resolved without HM two-way coupling. The Mandel effect is defined as further rapid groundwater level (i.e., hydraulic head or pore water pressure) rises as positive peaks immediately after its instantaneous rises in rectangular domains with a plane strain condition at the start of surface loading (e.g., Mandel 1953, Abousleiman *et al*. 1996). Cryer (1963) also presented a similar effect in spherical domains under uniform hydrostatic pressures, and it was called the Mandel-Cryer effect (e.g., Cryer 1963, Abousleiman *et al*. 1996). Such abnormal effects in rectangular domains have also been referred to as reverse (non-monotonic) groundwater level fluctuations because they are opposite to normal (monotonic) groundwater level responses in columnar domains (e.g., Section 4.1). The specific term Mandel was originated from the name of the scientist Mandel (1953) who first presented such reverse groundwater level fluctuations.

Mandel (1953) first proved analytically by deriving a HM analytical solution for the excess pore water pressure P_{ex} assuming no shear bending (no shear stress) that the Mandel effect is caused by distinct and unique hydro-mechanical responses of rectangular domains with plane strain conditions to mechanical surface loading stresses. The Mandel effect is caused by two mechanisms: plane strain condition perpendicular to the rectangular domain, and a faster mechanical propagation (compression) of the loading stress than its hydraulic propagation (pore water pressure decrease or head drawdown) from the surface (top boundary) to the center of the rectangular domain.

The physical settings including the assumptions and the initial and boundary conditions for this geomechanical validation problem are described in Appendix D. For such a case, Abousleiman *et al*. (1996) also derived a set of HM analytical solutions for the excess pore water pressure P_{ex}, horizontal displacement u_x, and vertical displacement u_z, whereas Mandel (1953) derived the HM analytical solution for the excess pore water pressure P_{ex} only, assuming no shear bending (no shear stress).

Only the vertically upper right quarter portion (i.e., shaded area) of the rectangle with its half width $a = W/2$ ($0 \leq x \leq +a$) and half height $b = H/2$ ($0 \leq z \leq +b$) is chosen to consider the lateral symmetries with respect to the horizontal x and vertical z axes (i.e., centerlines) in this geomechanical validation problem (Fig. 3). The half width $a = W/2$ and half height $b = H/2$ of the rectangle are set equal to 5 m and 10 m, respectively. Surface loading is applied on the top boundary (z = 10 m) at an instantaneous and constant total vertical normal stress σ_z = -10^6 N/m^2 (Pa). The material properties of the rectangle (fine sand) are obtained from the literature (Domenico and Schwartz 1990, Das 1994, Kim 2000) and are summarized in Table 1. The initial pore water pressure P_o at the horizontal x axis (i.e., centerline) (z = 0 m) is assigned to be equal to the half height of the rectangle multiplied by the unit weight of water (i.e., $P_o = b \times \gamma_w$ = 10 m × 9.81 × 10^3 N/m^3 = 9.81 × 10^4 N/m^2). The spatial and temporal discretizations used in the numerical simulation are described in Appendix D.

The sequentially coupled HM numerical solutions are plotted in Fig. 4 and compared with the HM analytical solutions (Mandel 1953, Abousleiman *et al*. 1996). As shown in Fig. 4, the numerical and analytical solutions show extremely or very good agreement for all the excess pore water pressure P_{ex}, horizontal displacement u_x, and vertical displacement u_z. In addition, as shown in Fig. 4(a), both numerical and analytical solutions for the excess pore water pressure clearly display the Mandel effect (i.e., positive peak immediately after the start of surface loading) at t = 140 sec. In Figs. 4(a) and 4(b), the coefficients of determination R^2 between the analytical and numerical solutions are 0.999, 0.996, and 0.994 for the temporal changes of the excess pore water pressure, horizontal displacement, and vertical displacement, respectively. In Figs. 4(c) and 4(d), the R^2 between the analytical and numerical solutions are 0.999, 0.997, and 0.998 for the spatial distributions of the excess pore water pressure, horizontal displacement, and vertical displacement, respectively.

5. Hydrogeological validation

5.1 Groundwater pumping from a single-layer confined aquifer

As the first hydrogeological validation problem, groundwater flow and land deformation (i.e., HM consolidation) in a saturated single-layer confined aquifer due to hydrological groundwater pumping, which are illustrated in Fig. 5, are simulated using the linked numerical model. Such sequentially coupled HM numerical solutions are then compared and validated with HM analytical solutions (verification).

The physical settings including the assumptions and the initial and boundary conditions for this hydrogeological validation problem are described in Appendix E. For such a case, Bear and Corapcioglu (1981) also derived a set of HM analytical solutions for the pore water pressure change ΔP,

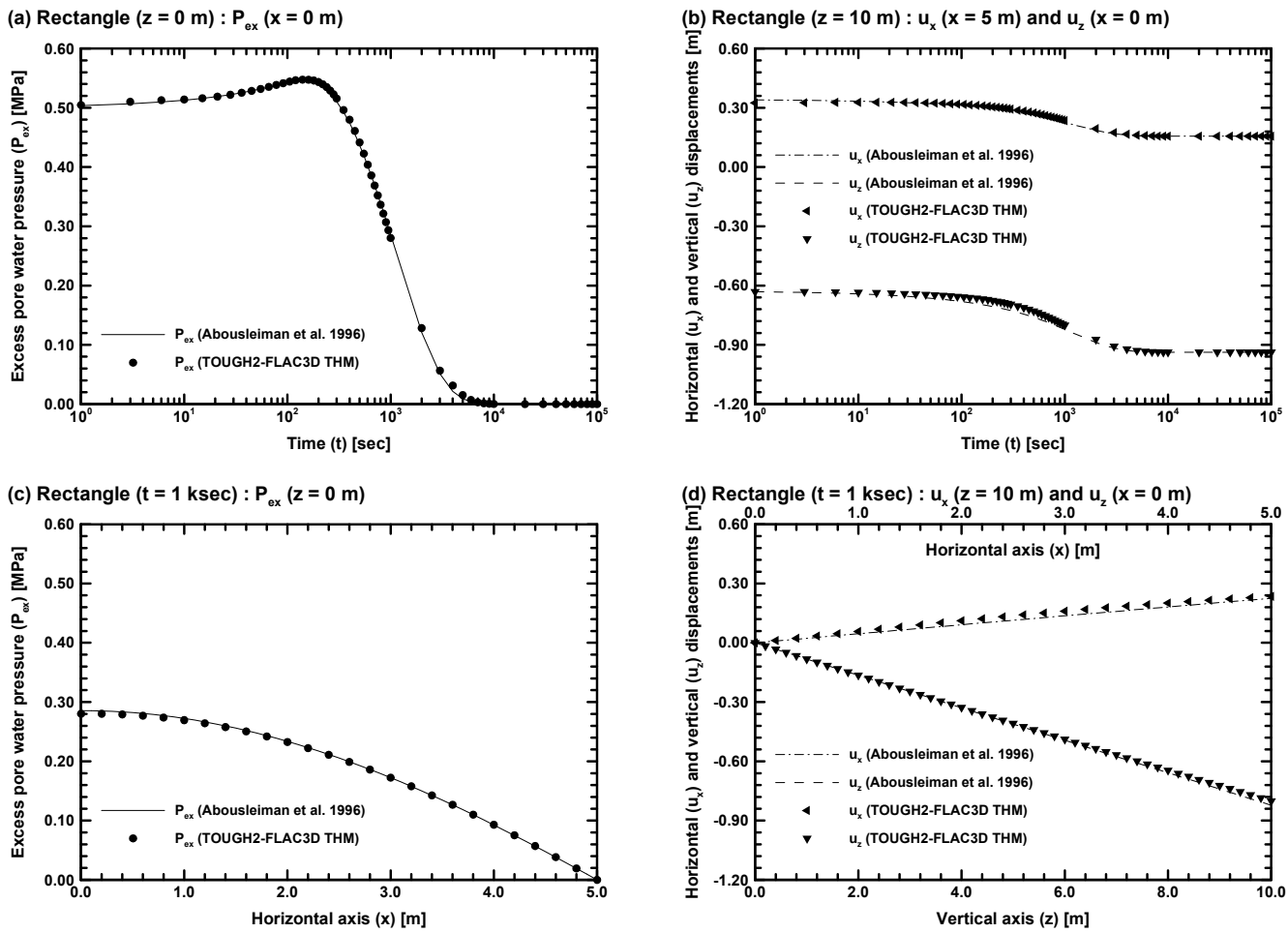

Fig. 4 Temporal changes (upper row) and spatial distributions (lower row) of (a) and (c) excess pore water pressure and (b) and (d) horizontal and vertical displacements in the saturated rectangle under surface loading

radial displacement u_r, and vertical displacement u_z.

Only the horizontally quarter portion (i.e., shaded area) of the single-layer confined aquifer with its tangential angle θ = 90° is chosen to consider the axial symmetry with respect to the vertical z axis (i.e., centerline) in this hydrogeological validation problem (Fig. 5). A radial extent of 300 km is chosen to approximate the infinite radial domain ($r_w \leq r \leq \infty$) of the single-layer confined aquifer, and its thickness B is set equal to 142 m. Groundwater is pumped from the single-layer confined aquifer through a fully penetrating pumping well with a radius r_w = 0.3 m at an instantaneous and constant rate Q_w = -1.0 m^3/sec = -1,000 kg/sec. The material properties of the single-layer confined aquifer (fractured rock) are obtained from the literature (Bear and Corapcioglu 1981, Kim and Parizek 1999) and are summarized in Table 2. The initial pore water pressure P_o at the bottom boundary (z = 0 m) is assigned to be equal to three times the thickness of the single-layer confined aquifer multiplied by the unit weight of water to avoid desaturation during the groundwater pumping (i.e., $P_o = 3 \times B \times \gamma_w = 3 \times 142$ m $\times$ 9.81 $\times$ 10^3 N/m^3 = 4.18 $\times$ 10^6 N/m^2). The spatial and temporal discretizations used in the numerical simulation are described in Appendix E.

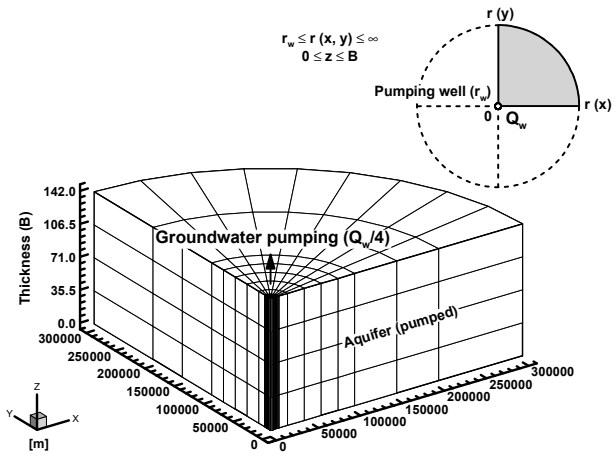

Fig. 5 Schematic diagram of the saturated single-layer confined aquifer under groundwater pumping and grid blocks used in the first hydrogeological validation problem

The sequentially coupled HM numerical solutions are plotted in Fig. 6 and compared with the HM analytical solutions (Bear and Corapcioglu 1981). As shown in Fig. 6, the numerical and analytical solutions show extremely or

Table 2 Material properties of the fractured rock used in the first hydrogeological validation problem

Property [unit]	Fractured rock (aquifer)
Porosity n [-]	0.10
Intrinsic permeability k [m^2]	6.82×10^{-12}
Saturated hydraulic conductivity K_{sat} [m/sec]	6.69×10^{-5}
Poisson's ratio ν [-]	0.25
Young's modulus E [Pa]	1.12×10^{8}
Biot's hydro-mechanical coupling coefficient α_c [-]	1.00
Solid density ρ_s [kg/m^3]	2.65×10^{3}

very good agreement for all the pore water pressure change ΔP, radial displacement u_r, and vertical displacement u_z. In Figs. 6(a) and 6(b), the coefficients of determination R^2 between the analytical and numerical solutions are 0.999, 0.998, and 0.997 for the temporal changes of the pore water pressure change, radial displacement, and vertical displacement, respectively. In Figs. 6(c) and 6(d), the R^2 between the analytical and numerical solutions are 0.999, 0.995, and 0.997 for the spatial distributions of the pore water pressure change, radial displacement, and vertical displacement, respectively.

5.2 Groundwater pumping on and off from a three-layer confined aquifer: Noordbergum and Rhade effects

As the second hydrogeological validation problem, groundwater flow and land deformation (i.e., HM consolidation) and the so-called Noordbergum and Rhade effects in a saturated three-layer confined aquifer (i.e., aquifer-aquitard system) due to hydrological groundwater pumping on and off, which are illustrated in Fig. 7, are simulated using the linked numerical model. Such sequentially coupled HM numerical solutions are then compared and validated with fully coupled HM numerical solutions (benchmarking).

The Noordbergum and Rhade effects are also phenomenally well-known but numerically challenging HM effects because they cannot be resolved without HM two-way coupling. The Noordbergum effect is defined as rapid groundwater level (i.e., hydraulic head or pore water pressure) rises as positive peaks in adjacent aquitards and unpumped aquifers to pumped aquifers immediately after the start of groundwater pumping (e.g., Barksdale *et al.* 1936, Ferris *et al.* 1962, Andreasen and Brookhart 1963,

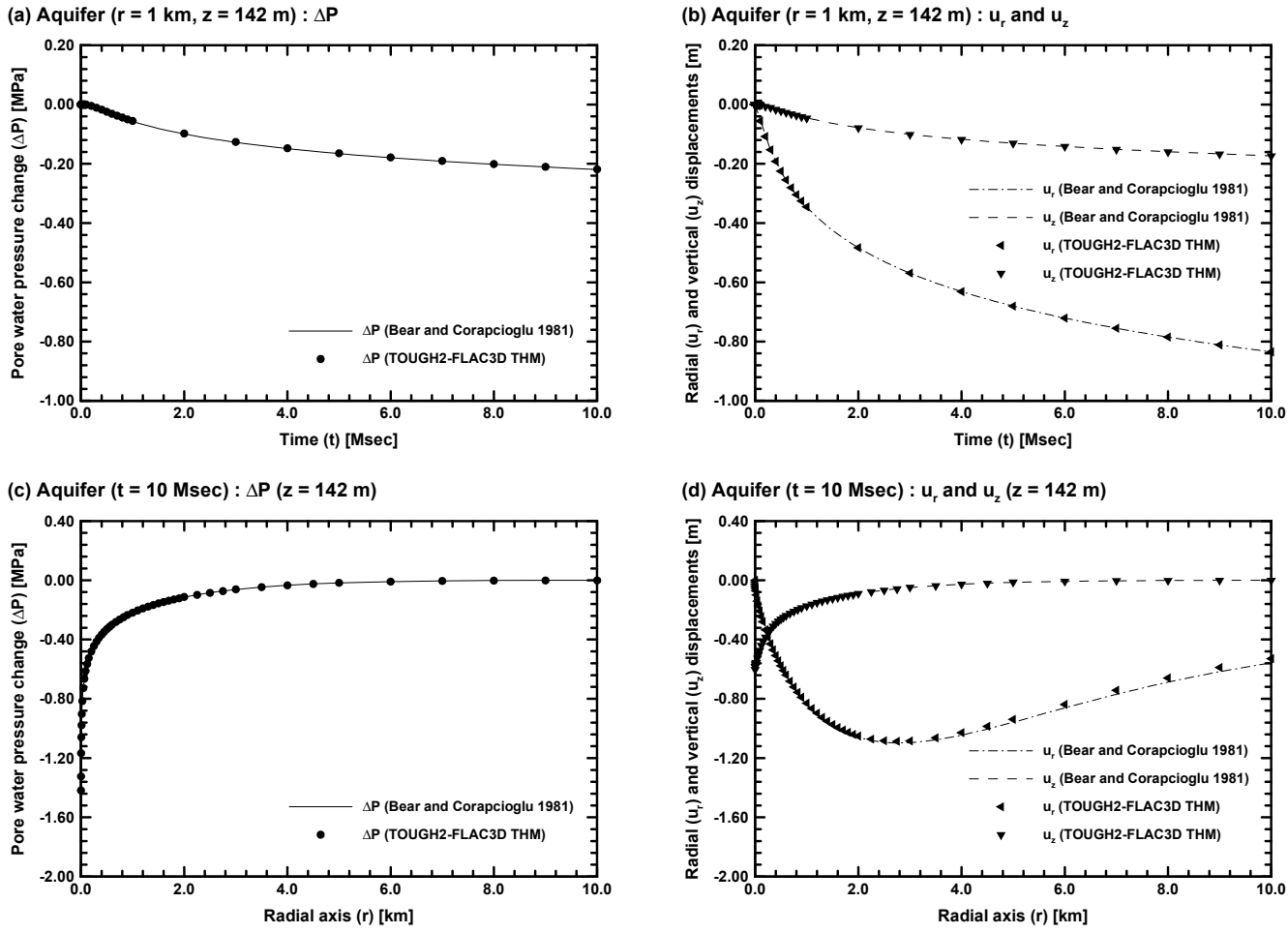

Fig. 6 Temporal changes (upper row) and spatial distributions (lower row) of (a) and (c) pore water pressure change and (b) and (d) radial and vertical displacements in the saturated single-layer confined aquifer under groundwater pumping

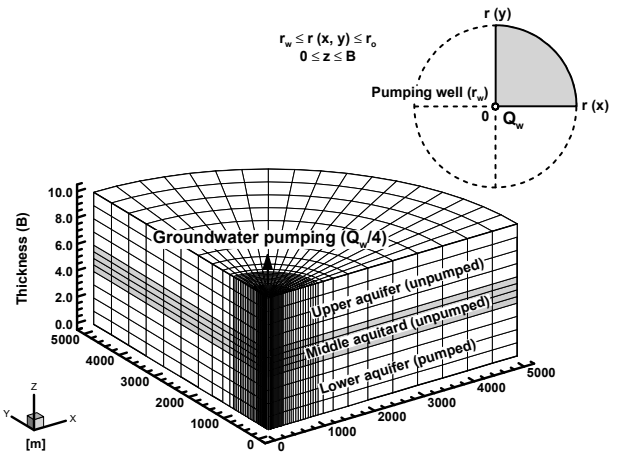

Fig. 7 Schematic diagram of the saturated three-layer confined aquifer under groundwater pumping on and off and grid blocks used in the second hydrogeological validation problem

van Eyden *et al*. 1964, Verruijt 1969, Wolff 1970a, 1970b, Rodrigues 1983, Langguth and Treskatis 1989, Broska and Barnette 1999). In the meantime, the Rhade effect is defined as rapid groundwater level (i.e., hydraulic head or pore water pressure) drops as negative peaks in adjacent aquitards and unpumped aquifers to pumped aquifers immediately after the end of groundwater pumping (e.g., Barksdale *et al*. 1936, van Eyden *et al*. 1964, Langguth and Treskatis 1989). Such abnormal effects in adjacent aquitards and unpumped aquifers have also been referred to as reverse (non-monotonic) groundwater level fluctuations because they are opposite to normal (monotonic) groundwater level responses in pumped aquifers (Andreasen and Brookhart 1963) (e.g., Section 5.1). The two specific terms Noordbergum and Rhade were originated from the names of the places where Verruijt (1969) and Langguth and Treskatis (1989) first observed such reverse groundwater level fluctuations, respectively.

Kim and Parizek (1997, 2005) first proved numerically by using a fully coupled HM numerical model COWADE123D (Kim 1995, 2002) that both Noordbergum and Rhade effects are caused by distinct and unique hydro-mechanical responses of layered heterogeneous aquifer-aquitard systems to hydrological groundwater pumping and unpumping stresses. The Noordbergum effect is caused by two mechanisms: a faster mechanical propagation (compression) of the pumping stress than its hydrological propagation (head drawdown or pore water pressure decrease) from the pumped aquifer into the adjacent aquitard due to its relatively lower hydraulic conductivity, and an amplification of the faster mechanical propagation (excessive compression) in the aquitard due to its relatively higher deformability. The Rhade effect is caused by two mechanisms: a slower hydrological propagation (head recovery or pore water pressure increase) of the unpumping stress than its mechanical propagation (extension) from the pumped aquifer into the adjacent aquitard due to its relatively lower hydraulic conductivity, and an amplification of the faster mechanical propagation (excessive extension) in the aquitard due to its relatively higher deformability.

The physical settings including the assumptions and the initial and boundary conditions for this hydrogeological validation problem are described in Appendix F. For such a case, the fully coupled HM numerical model COWADE123D (Kim 1995, 2002, 2006) is also used in order to obtain a set of fully coupled HM numerical solutions for the pore water pressure change ΔP, radial displacement u_r, and vertical displacement u_z.

Only the horizontally quarter portion (i.e., shaded area) of the three-layer confined aquifer with its tangential angle $\theta = 90°$ is chosen to consider the axial symmetry with respect to the vertical z axis (i.e., centerline) in this hydrogeological validation problem (Fig. 7). A radial extent of 5 km is chosen to represent the sufficiently large radial domain ($r_w \le r \le r_o$) of the three-layer confined aquifer, and its thickness B is set equal to 10 m. The three-layer confined aquifer consists of two 4-m-thick lower and upper aquifers, which are separated by a 2-m-thick middle aquitard, as an aquifer-aquitard system. Groundwater is pumped from the lower aquifer through a fully penetrating pumping well with a radius r_w = 0.3 m at an instantaneous and constant rate Q_w = -0.02 m^3/sec = -20 kg/sec for 1 day, and then the pump is shut off afterward. The material properties of the lower and upper aquifers (sand) and middle aquitard (clay) are obtained from the literature (Kim and Parizek 1997, 2005) and are summarized in Table 3. The initial pore water pressure P_o at the bottom boundary (z = 0 m) is assigned to be equal to three times the thickness of the three-layer confined aquifer multiplied by the unit weight of water to avoid desaturation during the groundwater pumping on and off (i.e., $P_o = 3 \times B \times \gamma_w$ = 3 × 10 m × 9.81 × 10^3 N/m^3 = 2.94 × 10^5 N/m^2). The spatial and temporal discretizations used in the numerical simulation are described in Appendix F.

The sequentially coupled HM numerical solutions are plotted in Fig. 8 and compared with the fully coupled HM numerical solutions (COWADE123D (Kim 1995, 2002, 2006)). As shown in Fig. 8, both numerical solutions show extremely good agreement for all the pore water pressure change ΔP, radial displacement u_r, and vertical displacement u_z. In addition, as shown in Fig. 8(c) (i.e.,

Table 3 Material properties of the sand and clay used in the second hydrogeological validation problem

Property [unit]	Sand (aquifer)	Clay (aquitard)
Porosity n [-]	0.44	0.66
Intrinsic permeability k [m^2]	9.24 × 10^{-11}	2.33 × 10^{-13}
Saturated hydraulic conductivity K_{sat} [m/sec]	9.06 × 10^{-4}	2.29 × 10^{-6}
Poisson's ratio ν [-]	0.25	0.35
Young's modulus E [Pa]	8.33 × 10^6	3.12 × 10^5
Biot's hydro-mechanical coupling coefficient α_c [-]	1.00	1.00
Solid density ρ_s [kg/m^3]	2.65 × 10^3	2.80 × 10^3

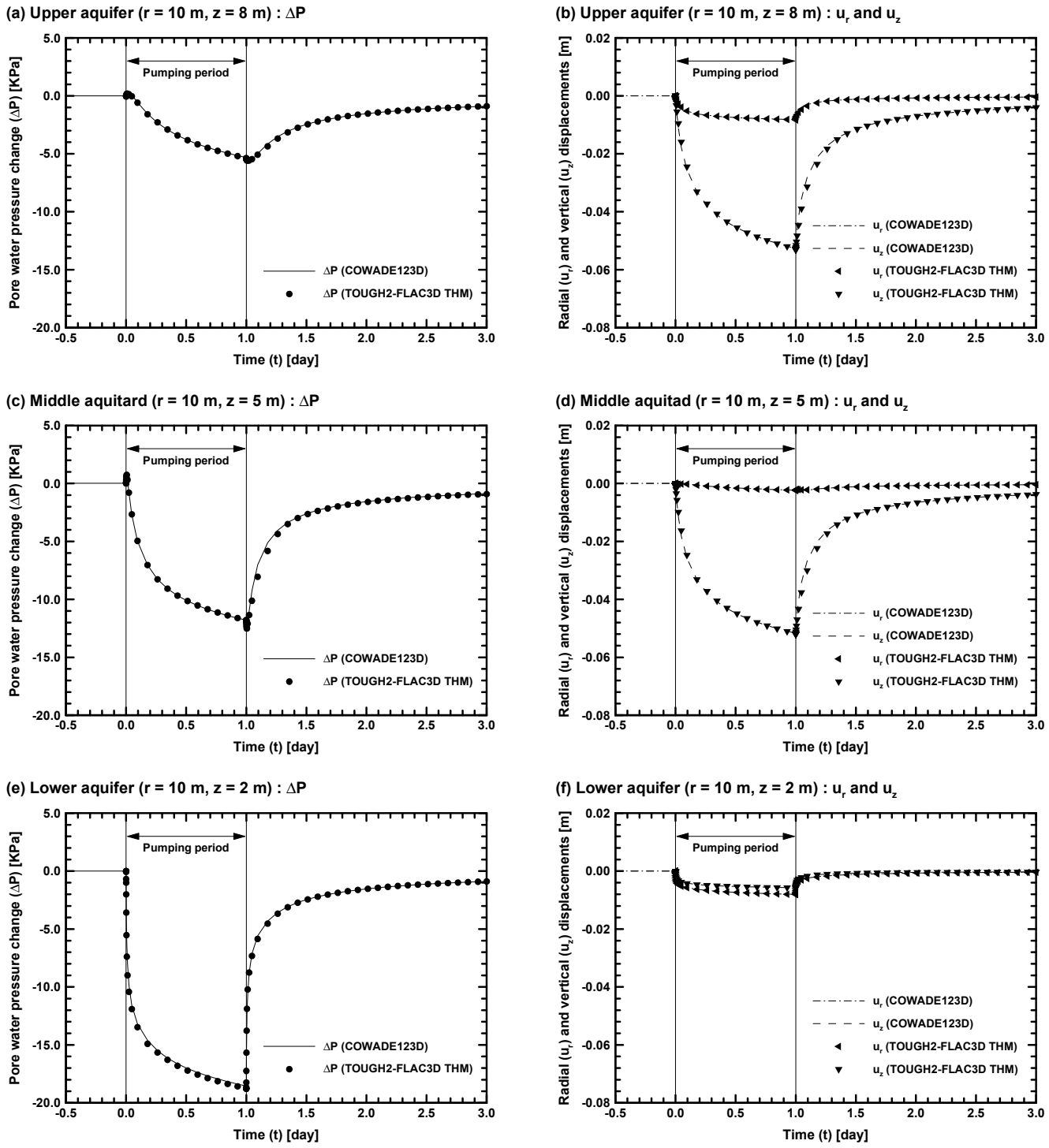

Fig. 8 Temporal changes of pore water pressure change (left column) and radial and vertical displacements (right column) in the (a) and (b) upper aquifer, (c) and (d) middle aquitard, and (e) and (f) lower aquifer at a radial distance of 10 m (r = 10 m) from the center of the saturated three-layer confined aquifer under groundwater pumping on and off

middle (unpumped) aquitard) and Fig. 8(a) (i.e., upper (unpumped) aquifer), both numerical solutions for the pore water pressure change clearly or slightly display the Noordbergum effect (i.e., positive peak immediately after the start of groundwater pumping) at t = 0 day and then the Rhade effect (i.e., negative peak immediately after the end of groundwater pumping) at t = 1 day. In Figs. 8(a) and 8(b), the coefficients of determination R^2 between both numerical solutions are 0.998, 0.999, and 0.997 for the temporal changes of the pore water pressure change, radial displacement, and vertical displacement, respectively, in the upper (unpumped) aquifer. In Figs. 8(c) and 8(d), the R^2 between both numerical solutions are 0.998, 0.999, and 0.997 for the temporal changes of the pore water pressure

change, radial displacement, and vertical displacement, respectively, in the middle (unpumped) aquitard. In Figs. 8(e) and 8(f), the R^2 between both numerical solutions are 0.999, 0.999, and 0.999 for the temporal changes of the pore water pressure change, radial displacement, and vertical displacement, respectively, in the lower (pumped) aquifer.

6. Discussions

The previous validation studies (e.g., Table 1 in Rutqvist (2017)) mainly concentrate on validation of the HM one- and two-way sequential coupling but less or even do not deal with validation of the TM and TH one- and two-way sequential coupling among the THM sequential coupling or linking (i.e., TOUGH2-FLAC3D linking algorithm) because of the following three main general reasons. First, the HM coupling is physically (i.e., linearly and nonlinearly) stronger and even mathematically more complicate than the TM and TH coupling among the THM (two-way sequential) coupling or linking (Kim 1996, Rutqvist *et al*. 2001, 2002, Rutqvist and Tsang 2003, Kim 2004, Rutqvist 2011, 2017). Second, thermal surface heating-induced one-dimensional TM expansion problems or thermal heat pumping-induced TM contraction problems are exactly mathematical analogues of mechanical surface loading-induced one-dimensional HM consolidation problems (e.g., Section 4.1) or hydrological groundwater pumping-induced HM consolidation problems (e.g., Section 5.1), respectively. Third, TH numerical solutions can be obtained only using a TH numerical model such as TOUGH2, and thus a coupled or linked THM numerical model is not necessary at all. This emphasizes the necessity for complete and successful validation of the HM two-way sequential coupling in the TOUGH2-FLAC3D linking algorithm in both M to H and H to M directions, which are initiated by mechanical surface loading (Section 4) and hydrological groundwater pumping (Section 5), respectively.

In the two geomechanical validation problems (Sections 4.1 and 4.2), the sequentially coupled numerical and analytical solutions show almost perfect to extremely or very good agreement for the excess pore water pressure, vertical displacement, and horizontal displacement. In the second geomechanical validation problem, the numerical and analytical solutions for the excess pore water pressure (i.e., Fig. 4(a)) also clearly display the Mandel effect (i.e., positive peak immediately after the start of surface loading). In addition, in the second geomechanical validation problem, the numerical solutions for the excess pore water pressure have significantly higher accuracy than those presented in the previous validation studies (TOUGH2-EGS (Fakcharoenphol *et al*. 2012, 2013, Hu *et al*. 2013), TOUGH2-CSM (THM-CO2) (Winterfeld *et al*. 2012, Winterfeld and Wu 2013, Huang *et al*. 2015, Winterfeld and Wu 2015, 2016), TOUGHREACT-ROCMECH (Kim *et al*. 2012a, 2012b, 2015), TOUGH+HYDRATE-FLAC3D (Kim *et al*. 2012c), and TOUGH+RealGasH2O-ROCMECH (Kim and Moridis 2013, 2014)). Most of the previous validation studies even did not present the numerical solutions for the vertical and horizontal displacements without rational reasons or clear explanations as mentioned in the introduction (Section 1). In other words, such previous validation studies were not perfectly successful. Some of the previous validation studies used zero value of Poisson's ratio and limited vertical grid discretization into only two layers as desperate measures to mitigate the shear bending at the top boundary (Kim *et al*. 2012a, Kim and Moridis 2013, Kim *et al*. 2015). It strongly implies either one or two aspects. One aspect is that the HM two-way sequential coupling scheme might not be implemented accurately into their TOUGH2- and TOUGHREACT-linked geomechanical numerical models. The other aspect is that they might overlook or underestimate the no shear bending (no shear stress) assumption used in derivation of the HM analytical solutions (Mandel 1953, Abousleiman *et al*. 1996) and thus establish improper numerical simulation setups. In the meantime, after a series of trial and error, this study finds that such a mathematical assumption is not applicable perfectly in the numerical simulation because the shear bending (shear stress) inevitably occurs at the top boundary and decreases with the downward direction to the center of the rectangle. As a result, the numerical and analytical solutions match best at the center of the rectangle but agree less with the upward direction from the center of the rectangle. In order to mitigate or minimize these deviations, a proper or minimum geometrical ratio (i.e., at least 2.0) of the height to the width is chosen and used for the rectangle after a series of trial and error in this study.

In the two hydrogeological validation problems (Sections 5.1 and 5.2), the sequentially coupled numerical and either analytical (Section 5.1) or fully coupled numerical (Section 5.2) solutions show extremely or very good to extremely good agreement for the pore water pressure change, vertical displacement, and radial displacement. In the second hydrogeological validation problem, both numerical solutions for the pore water pressure change (i.e., Figs. 8(c) and 8(a)) also clearly or slightly display the Noordbergum effect (i.e., positive peak immediately after the start of groundwater pumping) and then the Rhade effect (i.e., negative peak immediately after the end of groundwater pumping). Such hydrogeological validation problems have been absent so far since the first TOUGH2-linked geomechanical numerical model TOUGH-FLAC (Rutqvist *et al*. 2002, Rutqvist and Tsang 2003, Rutqvist 2011) was presented. Thus, this study first and successfully performs hydrogeological validation of a TOUGH2- or TOUGHREACT-linked geomechanical numerical model (i.e., HM two-way sequential coupling in the TOUGH2-FLAC3D linking algorithm). In addition, in the second hydrogeological validation problem, the extremely good agreement between both numerical solutions strongly suggests that the HM two-way sequential coupling scheme used in the linked numerical model is as rigorous as the HM two-way full coupling scheme used in

the fully coupled numerical model.

7. Conclusions

In this study, the hydro-mechanical (HM) two-way sequential coupling in the TOUGH2-FLAC3D linking algorithm was validated completely and successfully in both M to H and H to M directions, which were initiated by mechanical surface loading for geomechanical validation and hydrological groundwater pumping for hydrogeological validation, respectively. For such complete and successful validation, a TOUGH2-FLAC3D linked numerical model was developed first by adopting the TOUGH2-FLAC3D linking algorithm, which has been implemented in all the preexisting TOUGH2- and TOUGHREACT-linked geomechanical numerical models. In such TOUGH2-FLAC3D linking algorithm, the two-way (fixed-stress split) sequential coupling scheme and the implicit backward time stepping method were used. A series of four HM consolidation (groundwater flow and land deformation) problems was then simulated using the linked numerical model together with basic validation strategies and prerequisites. The former two were geomechanical validation problems induced by surface loading, and the latter two were hydrogeological validation problems caused by groundwater pumping. In particular, the second geomechanical and second hydrogeological validation problems were also associated with the Mandel effect and the Noordbergum and Rhade effects, respectively. These three are not only phenomenally well-known but also numerically challenging HM effects. Finally, sequentially coupled numerical solutions were compared with either analytical solutions (verification) or fully coupled numerical solutions (benchmarking). In all the four validation problems, they showed almost perfect to extremely or very good agreement. In addition, the second geomechanical validation problem clearly displayed the Mandel effect and suggested a proper or minimum geometrical ratio (i.e., at least 2.0) of the height to the width for the rectangular domain to maximize agreement between the numerical and analytical solutions. In the meantime, the second hydrogeological validation problem clearly displayed the Noordbergum and Rhade effects and implied that the HM two-way sequential coupling scheme used in the linked numerical model is as rigorous as the HM two-way full coupling scheme used in a fully coupled numerical model.

The above-mentioned conclusions of this study can be further summarized as the following research highlights: (1) the HM two-way sequential coupling in the TOUGH2-FLAC3D linking algorithm is first validated completely and successfully in both M to H and H to M directions, (2) a proper or minimum geometrical ratio of the height to the width is suggested for the rectangular domain to maximize agreement between the numerical and analytical solutions for the Mandel effect, and (3) the HM two-way sequential coupling is as rigorous as the HM two-way full coupling for the Noordbergum and Rhade effects.

Acknowledgments

This work was mainly supported by the Energy Efficiency and Resources Project funded by the Korea Institute of Energy Technology Evaluation and Planning (KETEP), Ministry of Trade, Industry and Energy (MOTIE), Korea under grant numbers 2010201020001A and GP2012-030. This work was also supported by the Korea CCS 2020 Project (Korea Carbon Capture and Sequestration R&D Center (KCRC)) funded by the National Research Foundation (NRF), Ministry of Science and Information and Communications Technology (MSIT), Korea under grant numbers 2013M1A8A1035824 and 2015M1A8A1048896. Sungho Lee was supported in part by the Brain Korea 21 Project funded by the National Research Foundation (NRF), Ministry of Science and Information and Communications Technology (MSIT), Korea. The authors would like to thank the Editor-in-Chief Professor Gye-Chun Cho at the Korea Advanced Institute of Science and Technology (KAIST) for handling this paper and the two anonymous reviewers for their invaluable and constructive review comments on this paper.

References

Abousleiman, Y., Cheng, A.H.D., Cui, L., Detournay, E. and Roegiers, J.C. (1996), "Mandel's problem revisited", *Géotechnique*, **46**(2), 187-195 (in English with French synopsis). https://doi.org/10.1680/geot.1996.46.2.187.

Aboustit, B.L., Advani, S.H., Lee, J.K. and Sandhu, R.S. (1982), "Finite element evaluations of thermo-elastic consolidation", in Goodman, R.E. and Hueze, F.E. (Editors), *Issues in Rock Mechanics: Proceedings of the 23rd Symposium on Rock Mechanics*, University of California, Berkeley, California, USA, August, Society of Mining Engineers, American Institute of Mining, Metallurgical and Petroleum Engineers, New York, New York, USA, 587-595.

Andreasen, G.E. and Brookhart, J.W. (1963), "Reverse water-level fluctuations", in Bentall, R. (Editor), "Methods of collecting and interpreting ground-water data", Water-Supply Paper No. 1544-H, United States Geological Survey, Denver, Colorado, USA, 30-35.

Barksdale, H.C., Sundstrom, R.W. and Brunstein, M.S. (1936), "Supplementary report on the ground-water supplies of the Atlantic City region", Special Report No. 6, New Jersey State Water Policy Commission, Trenton, New Jersey, USA, 139 pp.

Bear, J. and Corapcioglu, M.Y. (1981), "Mathematical model for regional land subsidence due to pumping, 2. Integrated aquifer subsidence equations for vertical and horizontal displacements", *Water Resour. Res.*, **17**(4), 947-958. https://doi.org/10.1029/WR017i004p00947.

Biot, M.A. (1941), "General theory of three-dimensional consolidation", *J. Appl. Phys.*, **12**(2), 155-164. https://doi.org/10.1063/1.1712886.

Biot, M.A. and Willis, D.G. (1957), "The elastic coefficients of the theory of consolidation", *J. Appl. Mech.*, *Trans. Am. Soc. Mech. Eng.*, **24**(4), 594-601. https://doi.org/10.1115/1.4011606.

Bishop, A.W. and Blight, G.E. (1963), "Some aspects of effective stress in saturated and partly saturated soils", *Géotechnique*, **13**(3), 177-197 (in English with French synopsis). https://doi.org/10.1680/geot.1963.13.3.177.

Broska, J.C. and Barnette, H.L. (1999), "Hydrogeology and

analysis of aquifer characteristics in west-central Pinellas County, Florida", Open-File Report No. 99-185, United States Geological Survey, Denver, Colorado, USA, 23 pp.

Carroll, M.M. (1979), "An effective stress law for anisotropic elastic deformation", *J. Geophys. Res. Solid Earth*, **84**(13), 7510-7512. https://doi.org/10.1029/JB084iB13p07510.

Carslaw, H.S. and Jaeger, J.C. (1959), *Conduction of Heat in Solids*, 2nd Edition, Oxford University Press, London, UK, 510 pp.

Cheng, A.H.D. (1997), "Material coefficients of anisotropic poroelasticity", *Int. J. Rock Mech. Min. Sci.*, **34**(2), 199-205. https://doi.org/10.1016/S0148-9062(96)00055-1.

COMSOL (2021), "COMSOL Multiphysics: A general-purpose simulation software for finite element analysis, version 6.0", Manual, COMSOL, Burlington, Massachusetts, USA, 14 volumes (Volume 1: Installation guide).

Cryer, C.W. (1963), "A comparison of the three-dimensional theories of Biot and Terzaghi", *Q. J. Mech. Appl. Math.*, **16**(4), 401-412. https://doi.org/10.1093/qjmam/16.4.401.

Das, B.M. (1994), *Principles of Geotechnical Engineering*, 3rd Edition, PWS Publishing Company, Boston, Massachusetts, USA, 672 pp.

Dassault Systèmes Simulia (2014), "Abaqus: A software suite for finite element analysis, version 6.14", Manual, Dassault Systèmes Simulia, Providence, Rhode Island, USA, 19 volumes (Volume 1: Abaqus/CAE user's guide).

Domenico, P.A. and Schwartz, F.W. (1990), *Physical and Chemical Hydrogeology*, John Wiley and Sons, New York, New York, USA, 824 pp.

Fakcharoenphol, P., Hu, L. and Wu, Y.S. (2012), "A fully-coupled fully-implicit flow and geomechanics model: Application for enhanced geothermal reservoir simulations", *Proceedings of the 37th Workshop on Geothermal Reservoir Engineering*, Stanford University, Stanford, California, USA, January-February, Technical Report No. SGP-TR-194, Stanford Geothermal Program, Stanford University, Stanford, California, USA, Paper No. Fakcharoenphol, 1-10.

Fakcharoenphol, P., Xiong, Y., Hu, L., Winterfeld, P.H., Xu, T. and Wu, Y.S. (2013), "User's guide of TOUGH2-EGS (TOUGH2-Enhanced Geothermal Systems): A coupled geomechanical and reactive geochemical simulator for fluid and heat flow in enhanced geothermal systems, version 1.0", Technical Report No. CSM-DE-EE0002762, Colorado School of Mines, Golden, Colorado, USA, 172 pp.

Ferris, J.G., Knowles, D.B., Brown, R.H. and Stallman, R.W. (1962), "Theory of aquifer tests", Water-Supply Paper No. 1536-E, United States Geological Survey, Denver, Colorado, USA, 174 pp.

Freeze, R.A. and Cherry, J.A. (1979), *Groundwater*, Prentice-Hall, Englewood Cliffs, New Jersey, USA, 604 pp.

Geertsma, J. (1957), "A remark on the analogy between thermoelasticity and the elasticity of saturated porous media", *J. Mech. Phys. Solids*, **6**(1), 13-16. https://doi.org/10.1016/0022-5096(57)90042-X.

Hu, L., Winterfeld, P.H., Fakcharoenphol, P. and Wu, Y.S. (2013), "A novel fully-coupled flow and geomechanics model in enhanced geothermal reservoirs", *J. Petrol. Sci. Eng.*, **107**, 1-11. https://doi.org/10.1016/j.petrol.2013.04.005.

Huang, Z.Q., Winterfeld, P.H., Xiong, Y., Wu, Y.S. and Yao, J. (2015), "Parallel simulation of fully-coupled thermal-hydro-mechanical processes in CO_2 leakage through fluid-driven fracture zones", *Int. J. Greenh. Gas Control*, **34**, 39-51. https://doi.org/10.1016/j.ijggc.2014.12.012.

Hurwitz, S., Christiansen, L.B. and Hsieh, P.A. (2007), "Hydrothermal fluid flow and deformation in large calderas: Inferences from numerical simulations", *J. Geophys. Res. Solid Earth*, **112**(2), B02206. https://doi.org/10.1029/2006JB004689.

Hutnak, M., Hurwitz, S., Ingebritsen, S.E. and Hsieh, P.A. (2009), "Numerical models of caldera deformation: Effects of multiphase and multicomponent hydrothermal fluid flow", *J. Geophys. Res. Solid Earth*, **114**(4), B04411. https://doi.org/10.1029/2008JB006151.

Itasca Consulting Group (1997), "FLAC3D: Fast Lagrangian analysis of continua in 3 dimensions, version 2.0", Manual, Itasca Consulting Group, Minneapolis, Minnesota, USA, 5 volumes (Volume 1: User's guide).

Itasca Consulting Group (2009), "FLAC3D: Fast Lagrangian analysis of continua in 3 dimensions, version 4.0", Manual, Itasca Consulting Group, Minneapolis, Minnesota, USA, 12 volumes (Volume 1: User's guide).

Itasca Consulting Group (2017), "FLAC3D: Fast Lagrangian analysis of continua in 3 dimensions, version 6.0", Manual, Itasca Consulting Group, Minneapolis, Minnesota, USA, 11 volumes (Volume 1: User's guide).

Jaeger, J.C., Cook, N.G.W. and Zimmerman, R.W. (2007), *Fundamentals of Rock Mechanics*. 4th Edition, Blackwell Publishing, Malden, Massachusetts, USA, 475 pp.

Kim, J. (2010), "Sequential methods for coupled geomechanics and multiphase flow", Ph.D. Dissertation, Stanford University, Stanford, California, USA, 248 pp.

Kim, J. and Moridis, G.J. (2013), "Development of the T+M coupled flow-geomechanical simulator to describe fracture propagation and coupled flow-thermal-geomechanical processes in tight/shale gas systems", *Comput. Geosci.*, **60**, 184-198. https://doi.org/10.1016/j.cageo.2013.04.023.

Kim, J. and Moridis, G.J. (2014), "Gas flow tightly coupled to elastoplastic geomechanics for tight- and shale-gas reservoirs: Material failure and enhanced permeability", *SPE J.*, **19**(6), 1110-1125. https://doi.org/10.2118/155640-PA.

Kim, J., Moridis, G.J., Yang, D. and Rutqvist, J. (2012c), "Numerical studies on two-way coupled fluid flow and geomechanics in hydrate deposits", *SPE J.*, **17**(2), 485-501. https://doi.org/10.2118/141304-PA.

Kim, J., Sonnenthal, E. and Rutqvist, J. (2012a), "A sequential implicit algorithm of chemo-thermo-poro-mechanics for fractured geothermal reservoirs", *Proceedings of the TOUGH Symposium 2012*, Lawrence Berkeley National Laboratory, University of California, Berkeley, California, USA, September, 275-282.

Kim, J., Sonnenthal, E.L. and Rutqvist, J. (2012b), "Formulation and sequential numerical algorithms of coupled fluid/heat flow and geomechanics for multiple porosity materials", *Int. J. Numer. Meth. Eng.*, **92**(5), 425-456. https://doi.org/10.1002/nme.4340.

Kim, J., Sonnenthal, E. and Rutqvist, J. (2015), "A sequential implicit algorithm of chemo-thermo-poro-mechanics for fractured geothermal reservoirs", *Comput. Geosci.*, **76**, 59-71. https://doi.org/10.1016/j.cageo.2014.11.009.

Kim, J., Tchelepi, H.A. and Juanes, R. (2011a), "Stability and convergence of sequential methods for coupled flow and geomechanics: Fixed-stress and fixed-strain splits", *Comput. Meth. Appl. Mech. Eng.*, **200**(13-16), 1591-1606. https://doi.org/10.1016/j.cma.2010.12.022.

Kim, J., Tchelepi, H.A. and Juanes, R. (2011b), "Stability and convergence of sequential methods for coupled flow and geomechanics: Drained and undrained splits", *Comput. Meth. Appl. Mech. Eng.*, **200**(23-24), 2094-2116. https://doi.org/10.1016/j.cma.2011.02.011.

Kim, J.M. (1995), "COWADE123D: A finite element model for fully coupled saturated-unsaturated water flow in deforming one-, two-, and three-dimensional porous and fractured media, version 1.0", Technical Report No. HGL-1995-9, Hydrogeology Laboratory, Department of Geosciences, Pennsylvania State University, University Park, Pennsylvania, USA, 254 pp.

Kim, J.M. (1996), "A fully coupled model for saturated-unsaturated fluid flow in deformable porous and fractured media", Ph.D. Dissertation, Pennsylvania State University, University Park, Pennsylvania, USA, 201 pp.

Kim, J.M. (2000), "Generalized poroelastic analytical solutions for pore water pressure change and land subsidence due to surface loading", *Geosci. J.*, **4**(2), 95-104. https://doi.org/10.1007/BF02910130.

Kim, J.M. (2002), "COWADE123D: A finite element model for fully coupled saturated-unsaturated water flow in deforming one-, two-, and three-dimensional porous and fractured media, version 2.11", Technical Report No. GGEL-2002-9, Geological and Groundwater Engineering Laboratory, School of Earth and Environmental Sciences, Seoul National University, Seoul, Korea, 304 pp.

Kim, J.M. (2004), "Fully coupled poroelastic governing equations for groundwater flow and solid skeleton deformation in variably saturated true anisotropic porous geologic media", *Geosci. J.*, **8**(3), 291-300. https://doi.org/10.1007/BF02910248.

Kim, J.M. (2006), "COWADE123D: A finite element model for fully coupled saturated-unsaturated water flow in deforming one-, two-, and three-dimensional true anisotropic porous, fractured, and fractured porous geologic media, version 2.17", Technical Report No. GGEL-2006-11, Geological and Groundwater Engineering Laboratory, School of Earth and Environmental Sciences, Seoul National University, Seoul, Korea, 298 pp.

Kim, J.M. and Parizek, R.R. (1997), "Numerical simulation of the Noordbergum effect resulting from groundwater pumping in a layered aquifer system", *J. Hydrol.*, **202**(1-4), 231-243. https://doi.org/10.1016/S0022-1694(97)00067-X.

Kim, J.M. and Parizek, R.R. (1999), "Three-dimensional finite element modelling for consolidation due to groundwater withdrawal in a desaturating anisotropic aquifer system", *Int. J. Numer. Anal. Meth. Geomech.*, **23**(6), 549-571. https://doi.org/10.1002/(SICI)1096-9853(199905)23:6<549::AID-NAG983>3.0.CO;2-Y.

Kim, J.M. and Parizek, R.R. (2005), "Numerical simulation of the Rhade effect in layered aquifer systems due to groundwater pumping shutoff", *Adv. Water Resour.*, **28**(6), 627-642. https://doi.org/10.1016/j.advwatres.2004.12.005.

Kolditz, O., Görke, U.J., Shao, H. and Wang, W. (Editors) (2012), *Thermo-Hydro-Mechanical-Chemical Processes in Fractured Porous Media: Benchmarks and Examples*, Lecture Notes in Computational Science and Engineering, Volume 86, Springer-Verlag, Berlin, Germany, 399 pp.

Kwon, S. and Lee, C. (2018), "THM analysis for an in situ experiment using FLAC3D-TOUGH2 and an artificial neural network", *Geomech. Eng.*, **16**(4), 363-373. https://doi.org/10.12989/gae.2018.16.4.363.

Langguth, H.R. and Treskatis, C. (1989), "Reverse water level fluctuations in semiconfined aquifer systems – "Rhade effect"", *J. Hydrol.*, **109**(1-2), 79-93. https://doi.org/10.1016/0022-1694(89)90008-5.

Lee, J., Min, K.B. and Rutqvist, J. (2015a), "TOUGH-UDEC simulator for the coupled multiphase fluid flow, heat transfer, and deformation in fractured porous media", in Hassani, F.P., Hadjigeorgiou, J. and Archibald, J. (Editors), *Innovations in Applied and Theoretical Rock Mechanics: Proceedings of the 13th ISRM (International Society for Rock Mechanics and Rock Engineering) International Congress of Rock Mechanics*, Montreal Congress and Exhibition Centre (Palais des Congrès), Montreal, Quebec, Canada, May, Paper No. ISRM-13CONGRESS-2015-231, 1-10.

Lee, S., Park, J.Y., Kihm, J.H. and Kim, J.M. (2015b), "TOUGH2-FLAC3D THM: An integrated numerical model for coupled multi-phase thermo-hydro-mechanical processes in porous, fractured, and fractured porous geologic media by one-way and two-way sequential coupling of TOUGH2 and FLAC3D, version 1.0", Technical Report No. GGEL-2015-9, Geological and Groundwater Engineering Laboratory, School of Earth and Environmental Sciences, Seoul National University, Seoul, Korea, 59 pp.

Lei, H., Xu, T. and Jin, G. (2015), "TOUGH2Biot – A simulator for coupled thermal-hydrodynamic-mechanical processes in subsurface flow systems: Application to CO_2 geological storage and geothermal development", *Comput. Geosci.*, **77**, 8-19. https://doi.org/10.1016/j.cageo.2015.01.003.

Love, A.E.H. (1944), *A Treatise on the Mathematical Theory of Elasticity*, 4th Edition (republication), Dover Publications, New York, New York, USA, 643 pp.

Mandel, J. (1953), "Consolidation des sols (étude mathématique)", *Géotechnique*, **3**(7), 287-299 (in French with English synopsis). https://doi.org/10.1680/geot.1953.3.7.287.

McTigue, D.F. (1986), "Thermoelastic response of fluid-saturated porous rock", *J. Geophys. Res. Solid Earth*, **91**(9), 9533-9542. https://doi.org/10.1029/JB091iB09p09533.

Noorishad, J., Tsang, C.F. and Witherspoon, P.A. (1984), "Coupled thermal-hydraulic-mechanical phenomena in saturated fractured porous rocks: Numerical approach", *J. Geophys. Res. Solid Earth*, **89**(B12), 10365-10373. https://doi.org/10.1029/JB089iB12p10365.

Nur, A. and Byerlee, J.D. (1971), "An exact effective stress law for elastic deformation of rock with fluids", *J. Geophys. Res.*, **76**(26), 6414-6419. https://doi.org/10.1029/JB076i026p06414.

Olivella, S., Gens, A., Carrera, J. and Alonso, E.E. (1996), "Numerical formulation for a simulator (CODE_BRIGHT) for the coupled analysis of saline media", *Eng. Comput.*, **13**(7), 87-112. https://doi.org/10.1108/02644409610151575.

Pan, P.Z., Rutqvist, J., Feng, X.T. and Yan, F. (2013), "Modeling of caprock discontinuous fracturing during CO_2 injection into a deep brine aquifer", *Int. J. Greenh. Gas Control*, **19**, 559-575. https://doi.org/10.1016/j.ijggc.2013.10.016.

Pan, P.Z., Rutqvist, J., Feng, X.T. and Yan, F. (2014a), "An approach for modeling rock discontinuous mechanical behavior under multiphase fluid flow conditions", *Rock Mech. Rock Eng.*, **47**(2), 589-603. https://doi.org/10.1007/s00603-013-0428-1.

Pan, P.Z., Rutqvist, J., Feng, X.T. and Yan, F. (2014b), "TOUGH-RDCA modeling of multiple fracture interactions in caprock during CO_2 injection into a deep brine aquifer", *Comput. Geosci.*, **65**, 24-36. https://doi.org/10.1016/j.cageo.2013.09.005.

Pruess, K. (1991), "TOUGH2 – A general-purpose numerical simulator for multiphase fluid and heat flow", Technical Report No. LBL-29400, Lawrence Berkeley Laboratory, University of California, Berkeley, California, USA, 102 pp.

Pruess, K., Oldenburg, C. and Moridis, G. (1999), "TOUGH2 user's guide, version 2.0", Technical Report No. LBNL-43134, Lawrence Berkeley National Laboratory, University of California, Berkeley, California, USA, 197 pp.

Pruess, K., Oldenburg, C. and Moridis, G. (2012), "TOUGH2 user's guide, version 2.0 (revised version)", Technical Report No. LBNL-43134, Lawrence Berkeley National Laboratory, University of California, Berkeley, California, USA, 197 pp.

Rodrigues, J.D. (1983), "The Noordbergum effect and characterization of aquitards at the Rio Maior mining project", *Ground Water*, **21**(2), 200-207. https://doi.org/10.1111/j.1745-6584.1983.tb00714.x.

Rutqvist, J. (2011), "Status of the TOUGH-FLAC simulator and recent applications related to coupled fluid flow and crustal deformations", *Comput. Geosci.*, **37**(6), 739-750. https://doi.org/10.1016/j.cageo.2010.08.006.

Rutqvist, J. (2017), "An overview of TOUGH-based geomechanics models", *Comput. Geosci.*, **108**, 56-63. https://doi.org/10.1016/j.cageo.2016.09.007.

Rutqvist, J., Börgesson, L., Chijimatsu, M., Kobayashi, A., Jing, L., Nguyen, T.S., Noorishad, J. and Tsang, C.F. (2001), "Thermohydromechanics of partially saturated geological media: Governing equations and formulation of four finite element models", *Int. J. Rock Mech. Min. Sci.*, **38**(1), 105-127. https://doi.org/10.1016/S1365-1609(00)00068-X.

Rutqvist, J. and Tsang, C.F. (2003), "TOUGH-FLAC: A numerical simulator for analysis of coupled thermal-hydrologic-mechanical processes in fractured and porous geological media under multi-phase flow conditions", *Proceedings of the TOUGH Symposium 2003*, Lawrence Berkeley National Laboratory, University of California, Berkeley, California, USA, May, 1-9.

Rutqvist, J., Wu, Y.S., Tsang, C.F. and Bodvarsson, G. (2002), "A modeling approach for analysis of coupled multiphase fluid flow, heat transfer, and deformation in fractured porous rock", *Int. J. Rock Mech. Min. Sci.*, **39**(4), 429-442. https://doi.org/10.1016/S1365-1609(02)00022-9.

Taron, J. (2009), "Geophysical and geochemical analyses of flow and deformation in fractured rock", Ph.D. Dissertation, Pennsylvania State University, University Park, Pennsylvania, USA, 183 pp.

Taron, J. and Elsworth, D. (2010), "Coupled mechanical and chemical processes in engineered geothermal reservoirs with dynamic permeability", *Int. J. Rock Mech. Min. Sci.*, **47**(8), 1339-1348. https://doi.org/10.1016/j.ijrmms.2010.08.021.

Taron, J., Elsworth, D. and Min, K.B. (2009), "Numerical simulation of thermal-hydrologic-mechanical-chemical processes in deformable, fractured porous media", *Int. J. Rock Mech. Min. Sci.*, **46**(5), 842-854. https://doi.org/10.1016/j.ijrmms.2009.01.008.

Taron, J., Min, K.B., Yasuhara, H., Trakoolngam, K. and Elsworth, D. (2006), "Numerical simulation of coupled thermo-hydro-chemo-mechanical processes through the linking of hydrothermal and solid mechanics codes", *Proceedings of the 41st US Rock Mechanics Symposium (Golden Rocks 2006)*, Colorado School of Mines, Golden, Colorado, USA, June, Volume 1, Paper No. ARMA/USRMS-06-1128, 268-276.

Terzaghi, K. (1925), *Erdbaumechanik auf Bodenphysikalischer Grundlage*, Franz Deuticke, Leipzig, Saxony, Germany, 399 pp (in German).

Thompson, M. and Willis, J.R. (1991), "A reformation of the equations of anisotropic poroelasticity", *J. Appl. Mech.*, *Trans. Am. Soc. Mech. Eng.*, **58**(3), 612-616. https://doi.org/10.1115/1.2897239.

van Eyden, W.A.A., Kuper, H.W. and Santema, P. (1964), "Some methods used in the geo-hydrologic survey of the south-western deltaic area in the Netherlands", in IAHS Red Books, Volume 63, *Proceeding of the Symposium on Surface Waters, 13th IUGG (International Union of Geodesy and Geophysics) General Assembly*, University of California, Berkeley, California, USA, August, 1963, International Association of Hydrological Sciences, Ghent, East Flanders, Belgium, 528-557.

Verruijt, A. (1969), "Elastic storage of aquifers", in De Wiest, R.J.M. (Editor), *Flow through Porous Media*, Academic Press, New York, New York, USA, 331-376.

Winterfeld, P.H. and Wu, Y.S. (2013), "User's guide for TOUGH2-CSM (TOUGH2-Carbon Sequestration Model): Massively parallel simulation of fully-coupled flow with geomechanics", Technical Report No. CSM-DE-FC26-09FE0000988, Colorado School of Mines, Golden, Colorado, USA, 151 pp.

Winterfeld, P.H. and Wu, Y.S. (2015), "Simulation of coupled thermal-hydrological-mechanical phenomena in porous and fractured media", *Proceedings of the 2015 SPE (Society of Petroleum Engineers) Reservoir Simulation Symposium*, Royal Sonesta Hotel-Houston Galleria, Houston, Texas, USA, February, Paper No. SPE-173210-MS, 1-15.

Winterfeld, P.H. and Wu, Y.S. (2016), "Simulation of coupled thermal/hydrological/mechanical phenomena in porous media", *SPE J.*, **21**(3), 1041-1049. https://doi.org/10.2118/173210-PA.

Winterfeld, P.H., Wu, Y.S., Pruess, K. and Oldenburg, C. (2012), "Development of an advanced thermal-hydrological-mechanical model for CO_2 storage in porous and fractured saline aquifers", *Proceedings of the TOUGH Symposium 2012*, Lawrence Berkeley National Laboratory, University of California, Berkeley, California, USA, September, 806-813.

Wolff, R.G. (1970a), "Field and laboratory determination of the hydraulic diffusivity of a confining bed", *Water Resour. Res.*, **6**(1), 194-203. https://doi.org/10.1029/WR006i001p00194.

Wolff, R.G. (1970b), "Relationship between horizontal strain near a well and reverse water level fluctuation", *Water Resour. Res.*, **6**(6), 1721-1728. https://doi.org/10.1029/WR006i006p01721.

Xu, T., Sonnenthal, E., Spycher, N. and Pruess, K. (2004), "TOUGHREACT user's guide: A simulation program for non-isothermal multiphase reactive geochemical transport in variably saturated geologic media", Technical Report No. LBNL-55460, Lawrence Berkeley National Laboratory, University of California, Berkeley, California, USA, 197 pp.

Xu, T., Sonnenthal, E., Spycher, N. and Pruess, K. (2006), "TOUGHREACT user's guide: A simulation program for non-isothermal multiphase reactive geochemical transport in variably saturated geologic media, version 1.2", Technical Report No. LBNL-55460, Lawrence Berkeley National Laboratory, University of California, Berkeley, California, USA, 200 pp.

Xu, T., Sonnenthal, E., Spycher, N. and Zheng, L. (2014), "TOUGHREACT V3.0-OMP reference manual: A parallel simulation program for non-isothermal multiphase geochemical reactive transport", Technical Report No. LBNL-DRAFT, Lawrence Berkeley National Laboratory, University of California, Berkeley, California, USA, 141 pp.

Xu, T., Spycher, N., Sonnenthal, E., Zheng, L. and Pruess, K. (2012), "TOUGHREACT user's guide: A simulation program for non-isothermal multiphase reactive transport in variably saturated geologic media, version 2.0", Technical Report No. LBNL-DRAFT, Lawrence Berkeley National Laboratory, University of California, Berkeley, California, USA, 240 pp.

CC

Appendix A. Two-way sequential coupling scheme in TOUGH2-FLAC3D linking algorithm

The coupling (looping) logic and procedure (Rutqvist *et al*. 2002, Rutqvist and Tsang 2003, Rutqvist 2011) used in the TOUGH2-FLAC3D linking algorithm is schematically illustrated in Fig. A1. In order to run this linking algorithm, input data (i.e., meshes, material properties, initial conditions, boundary conditions, and others) for both TOUGH2 and FLAC3D are all required. When the input data are ready, the linking algorithm initially reads the input data for TOUGH2. After the read and update, TOUGH2 initializes all values for the initial time step and then gives outputs (i.e., numerical solutions) for the multi-phase fluid pressures P_β and temperature T as well as for the multi-component fluid mass and heat energy transport fluxes (i.e., specific discharges) $\boldsymbol{F}^\kappa$ and $\boldsymbol{F}^h$, respectively. Subsequently, the linking algorithm reads the input data for FLAC3D and the initial bulk fluid pressure P_f, temperature T, and bulk density ρ_b from TOUGH2 by using the built-in command script FISH (FLAC-ISH), which is a semi-compiled programming language embedded within FLAC3D that enables users to define new variables and functions. According to isothermal or non-isothermal and body force considerations, the bulk fluid pressure, temperature, and bulk density are updated into FLAC3D by using FISH. After the read and update, FLAC3D initializes all values for the initial time step and then gives outputs (i.e., numerical solutions) for the mechanical displacement vector $\boldsymbol{u} = u_i$, strain tensor $\boldsymbol{\varepsilon} = \varepsilon_{ij}$, effective stress tensor $\boldsymbol{\sigma}' = \sigma'_{ij}$, and total stress tensor $\boldsymbol{\sigma} = \sigma_{ij}$ for the subscripts $i,j = x,y,z$. Here x, y, and z are taken as the fixed global Cartesian coordinate axes such that the z axis is vertically upward. As a result, the initial-state loop between TOUGH2 and FLAC3D finishes, and a steady- or transient-state loop between TOUGH2 and FLAC3D starts for a new time step like the above-mentioned initial-state loop. In the present time step loop, TOUGH2 uses the numerical solutions for the strain tensor or total stress tensor from FLAC3D at the previous time step as the previous mechanical values for the T and H governing equations (e.g., Eqs. (13), (14), and (19) in Rutqvist *et al*. (2001)), while FLAC3D uses the numerical solutions for the bulk fluid pressure, temperature, and bulk density from TOUGH2 at the present time step as the present hydrological and thermal values for the M governing equation (e.g., Eq. (21) in Rutqvist *et al*. (2001)). This present time step loop continues until TOUGH2 and FLAC3D sequentially satisfy convergence criteria and give new outputs (i.e., numerical solutions). In every new time step, both TOUGH2 and FLAC3D run in this manner, which is called the staggered two-way sequential coupling scheme (Rutqvist *et al*. 2002, Rutqvist and Tsang 2003, Rutqvist 2011, Kim *et al*. 2012a, 2012b, 2015) as shown in Fig. A2.

Note that the numerical solutions for the multi-phase fluid pressures P_β and temperature T are obtained at the centers of the grid blocks in the TOUGH2 simulation, whereas the numerical solution for the mechanical displacement vector $\boldsymbol{u} = u_i$ is obtained at the nodes of the grid blocks in the FLAC3D simulation (e.g., Fig. 1 in Rutqvist *et al*. (2002)). The numerical solutions for the multi-phase fluid pressures P_β and temperature T are then linearly interpolated into the nodes of the grid blocks in the TOUGH2-FLAC3D linking algorithm.

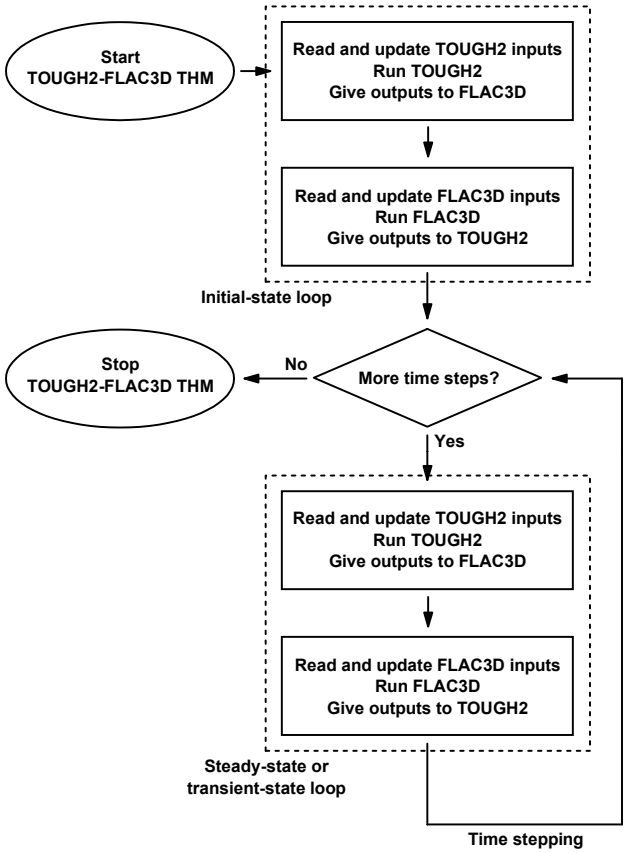

Fig. A1 Flow chart of coupling (looping) logic and procedure (Rutqvist *et al*. 2002, Rutqvist and Tsang 2003, Rutqvist 2011) used in the TOUGH2-FLAC3D linking algorithm

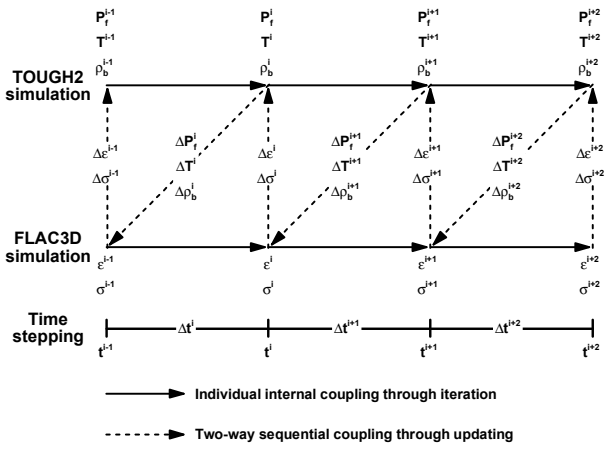

Fig. A2 Flow chart of staggered two-way sequential coupling scheme (Rutqvist *et al*. 2002, Rutqvist and Tsang 2003, Rutqvist 2011, Kim *et al*. 2012a, 2012b, 2015) used in the TOUGH2-FLAC3D linking algorithm

Appendix B. Implicit backward time stepping method with fixed-stress split scheme in TOUGH2-FLAC3D linking algorithm

In the M governing equation for a geologic medium (i.e., solid skeleton) (e.g., Eq. (21) in Rutqvist *et al*. (2001)), the total stress tensor term $\boldsymbol{\sigma} = \sigma_{ij}$ (positive for tension) can be defined in terms of the modified effective stress concept (Biot 1941, Biot and Willis 1957, Geertsma 1957, Bishop and Blight 1963, Nur and Byerlee 1971, Carroll 1979, McTigue 1986, Thompson and Willis 1991, Cheng 1997, Kim 2004) as follows:

$$\begin{aligned}\sigma_{ij} &= \sigma'_{ij} - \alpha_{c\,ij}\,P_f - \sigma'_{T\,ij} \\ &= D_{ijkl}\,\varepsilon_{kl} - \alpha_{c\,ij}\,P_f - D_{ijkl}\,\varepsilon_{T\,kl} \\ &= D_{ijkl}\,\varepsilon_{kl} - \alpha_{c\,ij}\,P_f - D_{ijkl}\,\gamma_{kl}\,T \\ &= D_{ijkl}\,\varepsilon_{kl} - \alpha_{c\,ij}\,P_f - \beta_{c\,ij}\,T \\ &\qquad\qquad i,j,k,l = x,y,z\end{aligned} \tag{B1}$$

where $\boldsymbol{\sigma}' = \sigma'_{ij} = D_{ijkl}\,\varepsilon_{kl}$ is the mechanical effective stress tensor (positive for tension) based on a generalized true anisotropic version of Hooke's law (Love 1944), $\boldsymbol{\alpha}_c = \alpha_{c\,ij} = \delta_{ij} - D_{ijkl}\,\delta_{kl}/3K_s$ is Biot's hydro-mechanical coupling or the effective stress coefficient tensor, $P_f = \sum S_\beta\,P_\beta$ is the bulk fluid pressure (positive for compression), $\boldsymbol{\sigma}'_T = \sigma'_{T\,ij} = D_{ijkl}\,\varepsilon_{T\,kl} = D_{ijkl}\,\gamma_{kl}\,T = \beta_{c\,ij}\,T$ is the thermal effective stress tensor (positive for compression), $\boldsymbol{D} = D_{ijkl}$ is the elastic modulus (stiffness) tensor, $\boldsymbol{\varepsilon} = \varepsilon_{kl} = \partial u_k/\partial x_l + (1-\delta_{kl})\,\partial u_l/\partial x_k$ is the mechanical strain tensor (positive for tension), $\boldsymbol{\varepsilon}_T = \varepsilon_{T\,kl} = \partial u_{T\,k}/\partial x_l + (1-\delta_{kl})\,\partial u_{T\,l}/\partial x_k$ is the thermal strain tensor (positive for compression), $\boldsymbol{\gamma} = \gamma_{kl}$ is the linear thermal expansion coefficient or expansivity tensor, $\boldsymbol{\beta}_c = \beta_{c\,ij} = D_{ijkl}\,\gamma_{kl}$ is the thermoelastic modulus (stiffness) or thermo-mechanical coupling coefficient tensor, and T is the temperature for the subscripts $i,j,k,l = x,y,z$. Here δ_{kl} is Kronecker's delta, $K_s = 1/\beta_s = E_s/[3(1-2\nu_s)]$ is the primary bulk modulus of the solid phase (i.e., solid grain) s with the micro-homogeneity and micro-isotropy assumptions, S_β is the saturation of the fluid phase β, P_β is the pressure of the fluid phase β (positive for compression), $\boldsymbol{u} = u_k$ is the mechanical displacement vector, and $\boldsymbol{u}_T = u_{T\,k}$ is the thermal displacement vector for the subscripts $k,l = x,y,z$. In addition, β_s is the primary compressibility, E_s is Young's modulus (modulus of elasticity), and ν_s is Poisson's ratio of the microscopically homogeneous and isotropic solid phase (i.e., solid grain) s.

As a result, in the T and H governing equations for a geologic medium (i.e., solid skeleton) (e.g., Eqs. (13), (14), and (19) in Rutqvist *et al*. (2001)), the temporal partial differential term of the mechanical strain tensor $\partial\varepsilon_{ij}/\partial t$ with Biot's hydro-mechanical coupling coefficient tensor $\alpha_{c\,ij}$ can then be defined using Eq. (B1) as follows:

$$\begin{aligned}\alpha_{c\,ij}\frac{\partial\varepsilon_{ij}}{\partial t} &= \alpha_{c\,ij}\,C_{ijkl}\frac{\partial\sigma'_{kl}}{\partial t} \\ &= \alpha_{c\,ij}\,C_{ijkl}\left(\frac{\partial\sigma_{kl}}{\partial t} + \alpha_{c\,kl}\frac{\partial P_f}{\partial t} + \frac{\partial\sigma'_{T\,kl}}{\partial t}\right) \\ &= \alpha_{c\,ij}\,C_{ijkl}\left(\frac{\partial\sigma_{kl}}{\partial t} + \alpha_{c\,kl}\frac{\partial P_f}{\partial t} + D_{klij}\,\gamma_{ij}\frac{\partial T}{\partial t}\right) \\ &= \alpha_{c\,ij}\,C_{ijkl}\left(\frac{\partial\sigma_{kl}}{\partial t} + \alpha_{c\,kl}\frac{\partial P_f}{\partial t} + \beta_{c\,kl}\frac{\partial T}{\partial t}\right) \\ &\qquad\qquad i,j,k,l = x,y,z\end{aligned} \tag{B2}$$

where $\boldsymbol{C} = C_{ijkl} = C_{klij} = \boldsymbol{D}^{-1} = D^{-1}_{klij} = D^{-1}_{ijkl}$ is the elastic compliance tensor.

In order to achieve unconditional stability and convergence of the two-way sequential coupling used in the TOUGH2-FLAC3D linking algorithm, Eq. (B2) can be transformed into a temporal difference form using the fixed-stress split scheme (Kim 2010, Kim *et al*. 2011a, 2011b) under the implicit backward (Euler) time stepping method as follows:

$$\begin{aligned}\alpha_{c\,ij}\frac{\Delta\varepsilon_{ij}}{\Delta t} &= \alpha_{c\,ij}\,C_{ijkl}\frac{\Delta\sigma'_{kl}}{\Delta t} \\ &= \alpha_{c\,ij}\,C_{ijkl}\left(\frac{\sigma^i_{kl}-\sigma^{i-1}_{kl}}{t^i-t^{i-1}} + \alpha_{c\,kl}\frac{P^{i+1}_f-P^i_f}{t^{i+1}-t^i} + \frac{\sigma'^{\,i+1}_{T\,kl}-\sigma'^{\,i}_{T\,kl}}{t^{i+1}-t^i}\right) \\ &= \alpha_{c\,ij}\,C_{ijkl}\left(\frac{\sigma^i_{kl}-\sigma^{i-1}_{kl}}{t^i-t^{i-1}} + \alpha_{c\,kl}\frac{P^{i+1}_f-P^i_f}{t^{i+1}-t^i} + D_{klij}\,\gamma_{ij}\frac{T^{i+1}-T^i}{t^{i+1}-t^i}\right) \\ &= \alpha_{c\,ij}\,C_{ijkl}\left(\frac{\sigma^i_{kl}-\sigma^{i-1}_{kl}}{t^i-t^{i-1}} + \alpha_{c\,kl}\frac{P^{i+1}_f-P^i_f}{t^{i+1}-t^i} + \beta_{c\,kl}\frac{T^{i+1}-T^i}{t^{i+1}-t^i}\right) \\ &\qquad\qquad i,j,k,l = x,y,z\end{aligned} \tag{B3}$$

where Δt is the time step size, and the superscripts $i-1$, i, and $i+1$ denote the three successive time steps in the discretized time domain (Fig. A2). Eq. (B3) acts as a coupling or correction equation between the strain tensor and either the effective stress or the total stress, bulk fluid pressure, and temperature within the T, H, and M governing equations.

For a mechanically and thermally isotropic geologic medium (i.e., solid skeleton) including the geomechanical (Section 4) and hydrogeological (Section 5) validation

problems, Eq. (B3) can be further expressed as follows:

$$\begin{aligned}\alpha_c\,\delta_{ij}\frac{\Delta\varepsilon_{ij}}{\Delta t}&=\alpha_c\frac{\Delta\varepsilon_v}{\Delta t}=\frac{\alpha_c}{K}\frac{\Delta\sigma'_m}{\Delta t}\\&=\frac{\alpha_c}{K}\left(\frac{\sigma_m^i-\sigma_m^{i-1}}{t^i-t^{i-1}}+\alpha_c\frac{P_f^{i+1}-P_f^i}{t^{i+1}-t^i}+\frac{\sigma'^{\,i+1}_{T\,m}-\sigma'^{\,i}_{T\,m}}{t^{i+1}-t^i}\right)\\&=\frac{\alpha_c}{K}\left(\frac{\sigma_m^i-\sigma_m^{i-1}}{t^i-t^{i-1}}+\alpha_c\frac{P_f^{i+1}-P_f^i}{t^{i+1}-t^i}+3\,K\,\gamma\frac{T^{i+1}-T^i}{t^{i+1}-t^i}\right)\\&=\frac{\alpha_c}{K}\left(\frac{\sigma_m^i-\sigma_m^{i-1}}{t^i-t^{i-1}}+\alpha_c\frac{P_f^{i+1}-P_f^i}{t^{i+1}-t^i}+\beta_c\frac{T^{i+1}-T^i}{t^{i+1}-t^i}\right)\\&\qquad i,j=x,y,z\end{aligned}\tag{B4}$$

where $\alpha_c=1-K/K_s=1-\beta_s/\beta$ is Biot's hydro-mechanical coupling or the effective stress coefficient, δ_{ij} is Kronecker's delta for the subscripts $i,j=x,y,z$, $\varepsilon_v=\varepsilon_{xx}+\varepsilon_{yy}+\varepsilon_{zz}$ is the mechanical volumetric strain (positive for tension), $K=1/\beta=E/[3(1-2\nu)]=(3\lambda+2\mu)/3$ is the bulk modulus, $\sigma'_m=\left(\sigma'_{xx}+\sigma'_{yy}+\sigma'_{zz}\right)/3$ is the mean confining mechanical effective stress (positive for tension), $\sigma_m=\left(\sigma_{xx}+\sigma_{yy}+\sigma_{zz}\right)/3$ is the mean confining total stress (positive for tension), $\sigma'_{T\,m}=\left(\sigma'_{T\,xx}+\sigma'_{T\,yy}+\sigma'_{T\,zz}\right)/3$ is the mean confining thermal effective stress (positive for compression), γ is the linear thermal expansion coefficient or expansivity, and $\beta_c=(3\lambda+2\mu)\,\gamma=3\,K\,\gamma$ is the thermoelastic modulus (stiffness) or thermo-mechanical coupling coefficient of the solid skeleton. Here $\beta=1/V\,(\partial V/\partial\sigma_m)_{P_f,T}\approx\partial\varepsilon_v/\partial\sigma'_m$ is the compressibility, E is Young's modulus (modulus of elasticity), ν is Poisson's ratio, and $\lambda=E\,\nu/[(1+\nu)(1-2\nu)]$ and $\mu=G=E/[2(1+\nu)]$ are Lame's first and second constants of the solid skeleton. In addition, V is the total volume, and G is the shear modulus (modulus of rigidity) of the solid skeleton.

Appendix C. HM consolidation in a saturated column due to surface loading

In the first geomechanical validation problem (Section 4.1), a saturated column under surface loading is considered as illustrated in Fig. 1. The column has a one-dimensional vertical columnar domain (z) with a vertical height H ($0\le z\le H$) and is under impermeable and full lateral restraint conditions in the lateral x and y directions perpendicular to the domain. Surface loading is applied on the top boundary ($z=H$) of the column at an instantaneous and constant (incremental) total vertical normal stress $\sigma_z=\sigma_{zz}$ (negative for compression). This situation is also equivalent to laterally uniform surface loading on a laterally infinite horizontal domain with a uniform thickness.

The column is assumed to be homogeneous and isotropic in space and time. Before the surface loading, the entire column is (pre)initially fully saturated up to its top boundary surface ($z=H$) and is at a hydrostatic equilibrium condition. During the surface loading, the permeable top boundary ($z=H$) maintains its initial pore water pressure by outward drainage, and it is free to move vertically. The impermeable bottom boundary ($z=0$) is fixed vertically. The whole column is confined laterally in a vertical impermeable and rigid frictionless sheath perpendicular to the domain so that groundwater flow and land deformation cannot occur laterally. As a result, the above-mentioned impermeable and full lateral restraint conditions maintain in the lateral x and y directions perpendicular to the domain.

The column (i.e., shaded area) is discretized into 100 hexahedral grid blocks (elements) of equal sizes (i.e., 1 × 1 × 100 in the lateral x and y and vertical z directions, respectively) with 404 nodes (i.e., 2 × 2 × 101 in the lateral x and y and vertical z directions, respectively) (Fig. 1). The vertical and lateral sizes of the grid blocks are set equal to 0.1 m, 1.0 m, and 1.0 m for 0 m $\le z\le$ 10 m, 0 m $\le x\le$ 1 m, and 0 m $\le y\le$ 1 m, respectively (i.e., Δz = 0.1 m and $\Delta x=\Delta y$ = 1.0 m). A maximum time step size of 10^3 sec and a total simulation time of 10^5 sec are used in the numerical simulation.

Appendix D. HM consolidation in a saturated rectangle due to surface loading

In the second geomechanical validation problem (Section 4.2), a saturated rectangle under surface loading is considered as illustrated in Fig. 3. The rectangle has a laterally symmetric two-dimensional vertical rectangular domain (x, z) with a horizontal width $W=2a$ ($-a\le x\le+a$) and a vertical height $H=2b$ ($-b\le z\le+b$) and is under impermeable and plane strain conditions in the lateral y direction perpendicular to the domain. Surface loading is applied on the top ($z=+b$) and bottom ($z=-b$) boundaries of the rectangle at an instantaneous and constant (incremental) total vertical normal stress $\sigma_z=\sigma_{zz}$ (negative for compression). This situation is also equivalent to laterally uniform surface loading on a laterally infinite horizontal and long domain perpendicular to it with a uniform thickness.

The rectangle is assumed to be homogeneous and isotropic in space and time. Before the surface loading, the entire rectangle is (pre)initially fully saturated up to its top boundary surface ($z=+b$) and is at a hydrostatic equilibrium condition. During the surface loading, the impermeable top boundary ($z=+b$) is free to move both vertically undistorted and horizontally considering a horizontal impermeable and rigid frictionless plate. The impermeable bottom boundary ($z=-b$) is also free to

move both vertically undistorted and horizontally considering an opposite horizontal impermeable and rigid frictionless plate. The permeable left ($x = -a$) and right ($x = +a$) boundaries maintain their initial pore water pressure by outward drainage, and they are free to move both vertically and horizontally. The whole rectangle is confined laterally between a pair of two horizontal impermeable and rigid frictionless plates perpendicular to the domain so that groundwater flow and land deformation cannot occur laterally. As a result, the above-mentioned impermeable and plane strain conditions maintain in the lateral y direction perpendicular to the domain.

The vertically upper right quarter portion (i.e., shaded area) of the rectangle is discretized into 1,250 hexahedral grid blocks (elements) of equal sizes (i.e., 25 × 1 × 50 in the horizontal x, lateral y, and vertical z directions, respectively) with 2,652 nodes (i.e., 26 × 2 × 51 in the horizontal x, lateral y, and vertical z directions, respectively) (Fig. 3). The vertical and lateral sizes of the grid blocks are set equal to 0.2 m, 0.2 m, and 1.0 m for 0 m $\leq z \leq$ 10 m, 0 m $\leq x \leq$ 5 m, and 0 m $\leq y \leq$ 1 m, respectively (i.e., $\Delta z = \Delta x$ = 0.2 m and Δy = 1.0 m). A maximum time step size of 10^3 sec and a total simulation time of 10^5 sec are used in the numerical simulation.

Appendix E. HM consolidation in a saturated single-layer confined aquifer due to groundwater pumping

In the first hydrogeological validation problem (Section 5.1), a saturated single-layer confined aquifer under groundwater pumping is considered as illustrated in Fig. 5. The single-layer confined aquifer has an axially symmetric three-dimensional cylindrical domain (r, z) with an infinite radial extent ($r_w \leq r \leq \infty$) and a vertical thickness B ($0 \leq z \leq B$). A vertical pumping well with a radius r_w fully penetrates through all the single-layer confined aquifer at the domain center ($r = 0$). The pumping well is then screened over the entire thickness of the single-layer confined aquifer. Groundwater is pumped from the single-layer confined aquifer through the pumping well at an instantaneous and constant rate Q_w (negative for pumping).

The single-layer confined aquifer is assumed to be homogeneous and isotropic in space and time. Before the groundwater pumping, the entire single-layer confined aquifer is (pre)initially fully saturated up to its top boundary surface ($z = B$) and is at a hydrostatic equilibrium condition. During the groundwater pumping, the inner pumping well bore boundary ($r = r_w$) is restrained from any radial displacement, but it is free to move vertically. The outer far-field concentric boundary ($r = \infty$) is not influenced by groundwater pumping, and it is free to move both vertically and radially. The impermeable bottom boundary ($z = 0$) is fixed vertically, but it is free to move radially. The impermeable top boundary ($z = B$) is free to move both vertically and radially.

The horizontally quarter portion (i.e., shaded area) of the single-layer confined aquifer is discretized into 2,016 hexahedral grid blocks (elements) of radially unequal sizes (i.e., 56 × 9 × 4 in the radial r, tangential θ, and vertical z directions, respectively) with 2,850 nodes (i.e., 57 × 10 × 5 in the radial r, tangential θ, and vertical z directions, respectively) (Fig. 5). The vertical and tangential sizes of the grid blocks are set equal to 35.5 m and 10° for 0 m $\leq z \leq$ 142 m and 0° $\leq \theta \leq$ 90°, respectively (i.e., Δz = 35.5 m and $\Delta\theta$ = 10°). A maximum time step size of 10^5 sec and a total simulation time of 10^7 sec are used in the numerical simulation.

Appendix F. HM consolidation in a saturated three-layer confined aquifer due to groundwater pumping on and off

In the second hydrogeological validation problem (Section 5.2), a saturated three-layer confined aquifer (i.e., aquifer-aquitard system) under groundwater pumping on and off is considered as illustrated in Fig. 7. The three-layer confined aquifer has an axially symmetric three-dimensional cylindrical domain (r, z) with a sufficiently large radial extent ($r_w \leq r \leq r_o$) and a vertical thickness B ($0 \leq z \leq B$). The three-layer confined aquifer consists of two lower and upper aquifers, which are separated by a middle aquitard, as an aquifer-aquitard system. A vertical pumping well with a radius r_w fully penetrates through all the three-layer confined aquifer at the domain center ($r = 0$). The pumping well is then cased throughout the whole thickness of the upper aquifer and middle aquitard, but it is screened over the entire thickness of the lower aquifer. Groundwater is pumped from the lower aquifer through the pumping well at an instantaneous and constant rate Q_w (negative for pumping) during a specific time period, and then the pump is shut off afterward.

Each of the lower and upper aquifers and middle aquitard is assumed to be homogeneous and isotropic in space and time. Before the groundwater pumping, the entire three-layer confined aquifer is (pre)initially fully saturated up to its top boundary surface ($z = B$) and is at a hydrostatic equilibrium condition. During the groundwater pumping on and off, the inner pumping well bore boundary ($r = r_w$) is restrained from any radial displacement, but it is free to move vertically. The outer far-field concentric boundary ($r = r_o$) is not influenced by groundwater pumping on and off, and it is free to move both vertically and radially. The impermeable bottom boundary ($z = 0$) is fixed vertically, but it is free to move radially. The impermeable top boundary ($z = B$) is free to move both vertically and radially.

The horizontally quarter portion (i.e., shaded area) of the three-layer confined aquifer is discretized into 13,176 hexahedral grid blocks (elements) of radially and vertically unequal sizes (i.e., 61 × 18 × 12 in the radial r, tangential θ, and vertical z directions, respectively) with 15,314 nodes (i.e., 62 × 19 × 13 in the radial r, tangential θ, and vertical z directions, respectively) (Fig. 7). The tangential sizes of the grid blocks are set equal to 5° for 0° $\leq \theta \leq$ 90° (i.e., $\Delta\theta$ = 5°). A maximum time step size of 3.6 × 10^3 sec (1 hour) and a total simulation time of 2.592 × 10^5 sec (3 days) are used in the numerical simulation.